NASA CONTRACTOR REPORT

NASA CR-2682

FLUID MECHANICAL MODEL OF THE ACOUSTIC IMPEDANCE OF SMALL ORIFICES

Alan S. Hersh and Thomas Rogers

Prepared by
HERSH ACOUSTICAL ENGINEERING
Chatsworth, Calif. 91311
for Lewis Research Center

NATIONAL AERONAUTICS AND SPACE ADMINISTRATION • WASHINGTON, D. C. • MAY 1976

1. Report No.	2. Government Accession No.	3. Recipient's
NASA CR-2682		

4. Title and Subtitle
FLUID MECHANICAL MODEL OF THE ACOUSTIC IMPEDANCE OF SMALL ORIFICES

5. Report Date
May 1976

6. Performing Organization Code

7. Author(s)
Alan S. Hersh and Thomas Rogers

8. Performing Organization Report No.
None

10. Work Unit No.

9. Performing Organization Name and Address
Hersh Acoustical Engineering
9545 Cozycroft Avenue
Chatsworth, California 91311

11. Contract or Grant No.
NAS3-17858

13. Type of Report and Period Covered
Contractor Report

12. Sponsoring Agency Name and Address
National Aeronautics and Space Administration
Washington, D.C. 20546

14. Sponsoring Agency Code

15. Supplementary Notes
Final Report. Project Manager, Edward J. Rice, V/STOL and Noise Division, NASA Lewis Research Center, Cleveland, Ohio

16. Abstract

A fluid mechanical model of the acoustic behavior of small orifices is presented which predicts orifice resistance and reactance as a function of incident sound pressure level, frequency, and orifice geometry. Agreement between predicted and measured values (in both water and air) of orifice impedance is excellent. The model shows the following: (1) The acoustic flow in the immediate neighborhood of the orifice (i.e., in the near field) can be modeled as a locally spherical flow. Within this near field, the flow is, to a first approximation, unsteady and incompressible. (2) At very low sound pressure levels, the orifice viscous resistance is directly related to the effect of boundary-layer displacement along the walls containing the orifice, and the orifice reactance is directly related to the inertia of the oscillating flow in the neighborhood of the orifice. Previously, orifice resistance and reactance were modeled by empirical end correction expressions. The model also shows that, at low to moderate sound pressure levels, the resistance can be dominated by weak nonlinear jet-like losses but that the overall impedance can still be constant (i.e., independent of incident sound pressure level) providing the orifice resistance is very small relative to the reactance. This is shown to occur when the amplitude of the incident acoustic pressure P is less than $\rho[\omega(D + L)]^2$, where ω is the sound radian frequency, D and L are the orifice diameter and thickness, respectively, and ρ is the fluid mean density. (3) When $P/\rho[\omega(D + L)]^2 >> 1$, the orifice impedance is dominated by nonlinear jet-like effects. This corresponds to very high sound pressure levels, at which the orifice behaves in a predominately quasi-steady manner. Thus, the model establishes explicitly the quasi-steady nature of the flow in orifices exposed to intense sound. (4) When $P/\rho[\omega(D + L)]^2 = 0$ (1), orifice resistance and reactance are roughly equal.

17. Key Words (Suggested by Author(s))	18. Distribution Statement
Sound absorbers; Acoustics; Nonlinear acoustic impedance; Acoustic impedance; Orifice flow	Unclassified - unlimited STAR Category 71

19. Security Classif. (of this report)	20. Security Classif. (of this page)	21. No. of Pages	22. Price*
Unclassified	Unclassified	56	$4.25

* For sale by the National Technical Information Service, Springfield, Virginia 22161

TABLE OF CONTENTS

SUMMARY

A fluid mechanical model of the acoustic behavior of small orifices is presented which predicts orifice resistance and *reactance* as a function of incident sound pressure level, frequency, and orifice geometry. Agreement between predicted and measured values (in both water and air) of orifice impedance is excellent. The model shows that

(1) The acoustic flow in the immediate neighborhood of the orifice (i.e., the near field) can be modeled as a locally spherical flow. Within this near field, the flow is, to a first approximation, unsteady and incompressible.

(2) At very low sound pressure levels, the orifice viscous resistance is directly related to the effect of boundary-layer displacement along the walls containing the orifice and the orifice reactance is directly related to the inertia of the oscillating flow in the orifice neighborhood. Previously, orifice resistance and reactance were modeled by empirical end correction expressions. The model also shows that at low to moderate sound pressure levels, the resistance can be dominated by weak nonlinear jet-like losses but that the overall impedance can still be constant (i.e., independent of incident sound pressure level) providing the orifice resistance is very small relative to the reactance. This is shown to occur when the amplitude of the incident acoustic pressure P is less than $\rho[\omega(D+L)]^2$ where ω is the sound radian frequency, (D+L) is the orifice diameter and thickness respectively and ρ is the fluid mean density.

(3) When $P/\rho[\omega(D+L)]^2>>1$, the orifice impedance is dominated by nonlinear jet-like effects. This corresponds to very high sound pressure levels at which the orifice behaves in a predominately quasi-steady manner. Thus the model establishes explicitly the quasi-steady nature of the flow in orifices exposed to intense sound.

(4) When $P/\rho[\omega(D+L)]^2=0(1)$, orifice resistance and reactance are roughly equal.

DEFINITION OF SYMBOLS

Symbol	Definition
A	constant defined by Eqn. (36)
A_i	airy function
c	speed of sound
C_D	time-averaged discharge coefficient
D	orifice diameter
f,g	special functions defined in text
F	special function defined in text
L	orifice thickness
L_o	radial distance of truncated hemispherical surface corresponding to orifice outlet
p	acoustic pressure
P	amplitude of incident acoustic pressure
r	radial distance
R	acoustic resistance
Re	orifice Reynolds number $(\omega^*(D^*+L^*)^2/\nu^*)$
t	time
u	radial velocity
V	maximum velocity at orifice vena contracta
V_i	orifice inlet velocity
X	orifice reactance
Z	orifice impedance
β	parameter defined as $\omega^*(D^*+L^*)/V^*$
ϵ	parameter defined as $V^*/\omega^*(D^*+L^*)$
δ	parameter defined as $\sqrt{2}\beta$
δ^*	boundary-layer displacement thickness
γ	ratio of specific heats
ν	fluid kinematic viscosity
μ	fluid coefficient of viscosity
ρ	fluid density
λ	sound wavelength
ω	sound radian frequency
θ	spherical polar angle (See Fig. 4a)
ζ	angle defined as $\pi/2-\theta$
ξ	transformed time coordinated (Eqn. 99)

Symbol	Definition
η	transformed boundary layer coordinate (Eqn. 54)
Δ_{NL}	nonlinear orifice end correction (Eqn. 2)

Superscripts

$( )^*$	denotes dimensional quantities
$(\bar{})^*$	denotes mean quantities

Subscripts

o	denotes lowest-order term
1	denotes first-order term; also harmonic term where obvious

1. INTRODUCTION

Cavity backed orifices are extensively used in the aircraft industry as acoustic devices to reduce or absorb internally generated jet engine machinery noise. The efficient application of these devices depends intimately upon the selection of the "optimum" impedance to maximize the sound absorption. The sound absorption theories of Morse[1] and Cremer[2] for rectangular ducts without flow show that the sound absorption decreases rapidly from its maximum value for off-optimum wall impedance. This sensitivity has also been shown by Rice[3] to exist for ducts containing flow. These studies demonstrate clearly the importance of accurately specifying the wall impedance in acoustically treated ducts.

Despite the extensive use of cavity-backed orifices in industry as devices to absorb undesired sound, their detailed acoustic behavior is not well understood. It has been shown by Ingard[4] and others that the absorption characteristics of these devices are directly related to their impedance. Thus, most acoustic studies of the behavior of cavity-backed orifices consist of the measurement and prediction of their impedance. The purpose of this report is to present a fluid mechanical model of the behavior of isolated small orifices as a function of incident sound pressure level, frequency, and orifice geometry. It is believed that this model will provide the necessary first step in understanding the behavior of cavity-backed orifices.

Rayleigh[5] was the first to predict the impedance of orifices by using the concept of lumped elements in a simple mechanical oscillator analogy (i.e., the slug-mass model). His model is essentially non-fluid mechanical but gives the actual acoustical impedance characteristics for low sound pressure levels when an empirical end correction is added to the slug mass. Rayleigh's model was modified first by Sirignano[6] and later by Zinn[7] by introducing fluid mechanical concepts. To simplify their models, they assumed that the characteristic dimensionsof both the orifice or cavity are very much smaller than the incident acoustic wavelength and, further, that the acoustic flow through the orifice is one-dimensional, incompressible, quasi-steady, and calorically perfect.

Both authors base their models on an integral formulation of the conservation of mass and momentum applied to two control volumes, one being the volume bounded by the orifice inlet and outlet surfaces and the other the cavity. To solve these integrals, they used the method of successive approximations with the first order solution corresponding to the linear case of very small sound pressures incident to an orifice. The orifice nonlinear behavior is introduced through the higher order terms and represent only a second order approximation to the (linear) first order solution. Thus their conclusions apply only to weakly nonlinear acoustic pressures and not to the intense sound pressures existing within rocket chambers or jet engines, the intended application of their models.

There is a serious deficiency common to both of their models. Sirignano assumes the loss in acoustic energy at the orifice outlet is equal to the jet outlet kinetic energy. Zinn assumes that, at

the orifice inlet, the axial inlet flow is zero but allows a radial inflow to preserve continuity. Both of these assumptions are difficult to understand because they violate their original assumptions. For example, Zinn's assumption that the flow in the orifice is one-dimensional (i.e., $\partial u/\partial x = 0$) clearly contradicts his zero inflow and jet-like outflow assumption. Sirignano violates the conservation of momentum by arbitrarily including a momentum term equal to $\gamma\rho u^2/2$ (see the third term on the RHS of Eqns. 10(a) and 10(b) of his paper). It is interesting to note that these two assumptions lead directly to a one-half difference in their estimate of the orifice nonlinear resistance. Another major deficiency of their models is that to first order (i.e., the so-called linear orifice impedance regime), both models predict the cavity resistance but *not* the orifice reactance.

Despite these criticisms, Sirignano and Zinn were the first to assume that the behavior of the nonlinear acoustic flow in the neighborhood of the orifice is quasi-steady and that the concept of a discharge coefficient properly connects the orifice inflow to the outflow.

Measurements of the behavior of small isolated orifices by Ingard and Ising[8] and by Thurston[9] et. al have provided valuable data and much needed physical insight. These studies are reviewed below because of their importance in the development of the fluid mechanical model described in Section 2.

Ingard and Ising used the arrangement shown in Figure 1 to study experimentally the acoustic nonlinearity of an isolated orifice. Figure 1 shows an orifice plate mounted at one end of a circular cylinder. The experimental program consisted of taking simultaneous measurements of the acoustic pressure within the cavity and the acoustic velocity in the orifice. The sound pressure level within the cavity was measured with a small condenser microphone. The acoustic velocity in the orifice was measured with a hot-wire probe placed at the center of the orifice. The air within the cavity was excited at a frequency of 150 Hz by means of an electromagnetically driven piston located at the bottom of the cavity.

The acoustic nonlinearity is described in terms of the behavior of the orifice impedance. Ingard and Ising defined the orifice impedance as the ratio of pressure within the cavity to the fundamental harmonic component of the orifice inlet velocity. The fundamental harmonic component of the orifice velocity was calculated by performing a Fourier decomposition of the measured orifice velocity time-history. The magnitude of the impedance is given by

$$Z^* = p_1^*/u_1^* \tag{1}$$

where p_1^* and u_1^* represent the amplitudes of the harmonic cavity pressure and orifice velocity respectively. The phase angle ϕ_1 between the acoustic pressure p_1^* and velocity u_1^* was determined

graphically by comparison of the pressure and velocity traces displayed simultaneously on an oscilloscope.

The results of their study are summarized in Figure 2 in terms of R^*, the orifice resistance, and X^* the orifice reactance. The data plotted against orifice inlet velocity, may be divided into two regions, one where $R^* << X^*$ and the other $R^* >> X^*$. In the region where $R^* << X^*$, the orifice impedance $Z^* \cong X^*$ is, to first order, constant independent of incident sound pressure level (and hence independent of orifice inlet velocity). In the region where $R^* >> X^*$, $Z^* \cong R^*$ and the data shows that, to first order, $R^* \sim \rho^* u_1^*$.

Ingard and Ising offer the following interpretation of their data. At low sound pressures (corresponding to $R^* << X^*$), the orifice resistance and reactance are given by the following empirical expressions

$$R^* \cong \sqrt{8\mu^*\rho^*\omega^*}\left(1 + L^*/D^* + \Delta_{NL}^*/D^*\right); \quad X \cong \rho^*\omega^*\left(L^* + 0.85\,D^*\right) \qquad (2a,b)$$

where L^* is the orifice plate thickness, D^* the diameter, Δ_{NL}^* the nonlinear resistive end correction, and $0.85D^*$ is the reactive mass end correction. These equations predict quite well the orifice impedance at these low sound pressure levels. The orifice inflow and outflow is essentially irrotational; the acoustic driving pressure is balanced primarily by the instantaneous (i.e., local) acceleration of the acoustic velocity in the vicinity of the orifice.

At high sound pressures (where $R^* >> X^*$), the measurements show (see Fig. 2) that the orifice resistance is proportional to the orifice velocity. The measurements also showed that the orifice reactance is very insensitive to orifice velocity, decreasing at the very highest sound pressure levels measured, to a value roughly one-half the linear value. Ingard and Ising interpreted the orifice resistance data in terms of Bernouilli's Law suggesting that the flow behavior through the orifice is quasi-steady. The hot-wire measurements indicated that at these high sound pressure levels, the flow separates at the orifice forming a high velocity jet. Thus during one-half cycle, the flow incident to the jet is irrotational; it is highly rotational (in the form of jetting) after exiting from the orifice. During the other half of the cycle, the flow pattern is reversed. The loss of one-half of the reactance at these high pressure levels was accounted for by assuming that one-half of the end correction is "blown" away by the exiting jet (in their experiments $L^*/D^* < 1$ hence from Eqn. 2 most of the reactance is due to the end correction). Ingard and Ising also measured the orifice velocity as a function of axial distance from the orifice (and away from the cavity - see Fig. 1). They found that the inflow velocity rapidly decayed to very small values at distances of about two to three diameters indicating that an acoustic near field existed.

In an earlier study, Thurston et. al measured the impedance of an isolated square-edged orifice of diameter 0.305 cm and, thickness 0.0126 cm immersed in water at temperature 26°C. The experimental set-up is quite similar to that used by Ingard and Ising consisting of a slender cylinder with a piston driver located at one end and the orifice at the opposite end. The acoustic pressure in the cavity was monitored with a capacitive type pressure detector and the acoustic velocity, generated by a piston-driver, was measured by means of a calibrated velocity pick-up attached to the drive shaft. The sinusoidal velocity at the orifice was calculated rather than measured by assuming that the sinusoidal volume velocity generated by the piston was equal to the sinusoidal volume velocity through the orifice. This relationship was assumed to be justified because of the stiffness of the cylinder walls and the relatively high incompressibility of water. Most of the measurements were conducted at a frequency of 22 Hz. In addition to the sinusoidal velocity source, a steady-state velocity was introduced by means of a needle valve connected to a high pressure source.

The results of Thurston's et. al orifice impedance measurements are shown in Figure 3. The shapes of both the orifice resistance and reactance curves are very similar to that of the Ingard and Ising's data (see Fig. 2) with the exception of the slight increase of reactance with orifice velocity at the higher orifice values. The agreement between the shapes of the resistance and reactance curves shown in Figures 2 and 3 is very impressive and lends added plausibility to Thurston's et. al assumption that for water the orifice velocity may be deduced by using the law of conservation of the sinusoidal volume velocity rather than by direct measurement.

2. MODEL OF THE ACOUSTICAL BEHAVIOR OF SMALL ORIFICES

A new fluid mechanical model of the acoustic behavior of small orifices is described below. The model is new because it differs in three fundamental ways from the earlier models of Sirignano and Zinn. The new assumptions are:

(1) The sound field incident to the orifice is assumed to be spherical rather than one dimensional as assumed by Sirignano and Zinn. This assumption provides the mechanism to connect unambiguously the relationship between the driving pressure incident to the orifice and the magnitude and relative phase of the orifice velocity. The models of Sirignano and Zinn proved deficient in this respect. For this assumption to be valid the orifice diameter must be very small relative to the incident sound wave length.

(2) Large changes in the magnitude and phase of the acoustic quantities are assumed to occur in the immediate neighborhood of the orifice. The hot-wire measurements conducted by Ingard and Ising of the acoustic velocity in the immediate neighborhood of the orifice show that it decreased significantly from its value at the orifice inlet within a distance of about two to three orifice diameters. This suggests immediately from the theory of ideal point

acoustic sources that the flow near the orifice should behave as an unsteady incompressible flow field (providing of course, that the velocity at the orifice outlet is small relative to the local speed of sound).

(3) The relationship between the sound pressure incident to the orifice and the resulting orifice outlet velocity is scaled according to whether the orifice impedance is constant ($R^* << X^*$) or varies linearly with orifice velocity ($R^* >> X^*$). The orifice impedance measurements conducted by Ingard and Ising and Thurston, et. al provide this relationship directly.

2.1 Approach

The analysis starts with the equations describing the conservation of mass and momentum written in spherical coordinates where only a radial *inward* flow u is assumed. For orifices small compared to the incident sound wavelength it is logical to assume that the flow approaches the orifice primarily in a spherical manner. The origin of the coordinate system is assumed to be located somewhere in the orifice interior as sketched in Figure 4. Assuming spherical symmetry, the flow field incident to the orifice will be assumed to be independent of the azimuthal angle ϕ (defined in Figure 4a). The flow field contains a uniform steady-state part and an oscillating acoustic part. A key element of the proposed model is the use of the experimental data of Thurston et. al and Ingard and Ising to normalize the equations describing the conservation of mass and radial momentum of the oscillating flow field. The experimental data shows that two distinct regimes exist; the regimes are defined by the relationships that exist between the amplitudes of the incident driving acoustic pressure P^* and the resulting amplitude of the acoustic velocity V^* in the orifice. For sufficiently low values of P^*, the data showed that

$$P^* \sim V^* \tag{3}$$

and for sufficiently high values of P^*;

$$P^* \sim (V^*)^2 \tag{4}$$

where $(\ )^*$ denotes that the term within the brackets is dimensional. The regime whose P^*, V^* relationship is characterized by Eqn. (3) is often called the linear regime while the regime characterized by Eqn. (4) is called the nonlinear regime.

It is clear from dimensional analysis that the proportionality term in Eqn. (3) must have dimensions of density times velocity while that of Eqn. (4) must be density. The only density term suggested by the physics of the flow is ρ^*, the mean fluid density. Thus, for orifices exposed to intense sound levels, the nonlinear case described above, the relationship characterizing P^* and V^* is

$$P^* = \rho^* (V^*)^2 \tag{4a}$$

At low sound pressure levels both Ingard and Ising's and Thurston's et. al. measurements show that the orifice impedance is dominated by the reactance X (see Figures 2 and 3), where X may be written (see Eqn. 2b)

$$X^* = \rho^* \omega^* (L^* + 0.85 D^*)$$

Since $|\dot{X}^*| >> |R^*|$ (and thus $P^*/V^* = Z^* \simeq X^*$ for most practical applications), where R^* is the orifice acoustical resistance, P^* is related to V^* as follows

$$P^* = \rho^* \omega^* (D^* + L^*) V^* \tag{3a}$$

where D^* and L^* represent the orifice diameter and thickness respectively. Equation (3a) can also be deduced from a dimensional argument. If viscosity plays a negligible role in affecting orifice reactance (suggested by the success of Rayleigh's slug mass model in predicting orifice reactance) then the only other available combination is $\omega^*(D^*+L^*)$.

Equation (3a) suggests that at low sound pressure levels where $P^* = Z^*V^* \simeq X^*V^*$ that

$$X^* = \rho^* \omega^* (D^* + L^*) \tag{5}$$

Figure 5 shows that orifice reactance does indeed behave according to Eqn. (5); the experimental data of Ingard and Ising and Thurston et. al. collapses into a single correlation curve. This agreement is remarkable when one considers the vast differences between these experiments. Ingard and Ising's measurements were conducted with an orifice diameter of 0.7 cm. in *air* exposed to sound frequency of 150 Hz while Thurston's et. al. measurements were conducted

with an orifice diameter of 0.3 cm. in *water* exposed to sound frequency of 22 Hz. Figure 5 shows that when $V^* = \omega^*(D^*+L^*)$, orifice reactance and resistance are (roughly) equal. Further, when $V^* < \omega^*(D^*+L^*)$, then $R^* << X^*$, the so-called linear regime, and when $V^* >> \omega^*(D^*+L^*)$, then $R^* >> X^*$, the nonlinear regime. We will show below that the ratio $V^*/\omega^*(D^*+L^*)$ is an important parameter in the development of the analytical model, and provides a means of separating the two regimes.

The successful correlation shown in Figure 5 of otherwise very dissimilar data suggest that P^*, V^*, D^*+L^*, $(\omega^*)^{-1}$ are the appropriate quantities that characterize the changes to the flow field near the orifice due to the sound. Recalling that the sound field incident to the orifice is assumed to be spherical, the solution to the (spherical) equations of motion governing the conservation of mass and radial momentum can be vastly simplified by proper scaling of the various terms and retaining only those of importance. The idea here is to try to anticipate the order of magnitude of the changes of the various terms in order to properly normalize them. If done correctly (and here the above correlation serves as a guide), then all of the dimensionless terms are of order unity and therefore may be rank-ordered in terms of their relative importance by the relative magnitude of their coefficients.

To start with, we will assume that changes in acoustic density are adabatically related to changes in acoustic pressure. Thus we write $\partial p^*/\partial \rho^* = c^{*2}$ The other quantities will be nondimensionalized letting

P^*	characterize	the	acoustic	pressure	change	near	the	orifice
ρ^*	"	"	"	density	"	"	"	"
V^*	"	"	"	velocity	"	"	"	"
(D^*+L^*)	"	"	"	length scale	"	"	"	"
$(\omega^*)^{-1}$	"	"	"	time scale	"	"	"	"

By defining the characteristic length as (D^*+L^*) rather than D^*, the effects of finite orifice thickness will be included in the model. In the derivation that follows, we assume that $L^* << D^*$.

Now introduce the nondimensional variables r, t, u, p, ρ.

$$r^* = (D^*+L^*)r,\ t^* = (\omega^*)^{-1}t,\ u^* = V^*u,\ p^* = P^*p,\ \rho^* = \frac{P^*}{(c^*)^2}\ \rho = \frac{P^*}{\rho^*(c^*)^2}\ \rho \qquad (6)$$

The last inequality on the R.H.S. of Eqn. (6) follows from the adiabatic relationship $p^* = (c^*)^2\rho^*$. Substituting Eqn. (6) into the conservation equations yields the following, the details of which are in the Appendix,

$$\left[\frac{P^*}{\rho^* c^{*2}}\right]\left[\frac{\omega^*(D^*+L^*)}{V^*}\right] r^2 \frac{\partial p}{\partial t} + \frac{\partial}{\partial r}(r^2 u) + \left[\frac{P^*}{\rho^* c^{*2}}\right] \frac{\partial}{\partial r}(\rho u r^2) = 0 \quad (7)$$

$$\left[\frac{\omega^*(D^*+L^*)}{V^*}\right] \frac{\partial u}{\partial t} + u \frac{\partial u}{\partial r} + \left[\frac{P^*}{\rho^* V^{*2}}\right]\left[1-\left(\frac{P^*}{\rho^* c^{*2}}\right) P\right] \frac{\partial p}{\partial r}$$

$$-\left[\frac{\nu^*}{V^*(D^*+L^*)}\right]\left[\frac{1}{r^2} \frac{\partial}{\partial r}(r^2 u) - \frac{2u}{r^2} + \frac{1}{r^2 \sin\Theta} \frac{\partial}{\partial \Theta}\left(\sin\Theta \frac{\partial u}{\partial \Theta}\right)\right] = 0 \quad (8)$$

$$\left[1-\left(\frac{P^*}{\rho^* c^{*2}}\right) P\right] \frac{\partial p}{\partial \Theta} - \left[\frac{2\nu^* \rho^* V^*}{P^*(D^*+L^*)}\right] \frac{1}{r} \frac{\partial u}{\partial \Theta} = 0 \quad (9)$$

The importance of the various terms in Eqns. (7), (8), and (9) are determined solely by the magnitude of their coefficients (recall that the non-dimensional terms have been normalized to be of order unity). To rank order these terms, the model is divided into the linear regime corresponding to low values of sound amplitude where $P^* = \rho^* \omega^* (D^*+L^*) V^*$ and the nonlinear regime corresponding to high amplitudes where $P^* = \rho^* V^{*2}$. From Figure 5, we see that at low values of P^*, $R^* << X^*$ and $V^* << \omega^*(D^*+L^*)$. Conversely, at high values of P^*, $R^* >> X^*$ and $V^* >> \omega^*(D^*+L^*)$. It follows from our initial assumption that the orifice diameter is very much less than the incident acoustic wavelength ($D^*+L^* << \lambda^*$), that therefore $\omega^*(D^*+L^*) << c^*$. Further, since the amplitude of the acoustic pressure will always be very much less than the ambient static pressure, it also follows that $V^* << c^*$.

Based on the above information, we can now rank order the relative importance of the various terms in Eqns. (7), (8), and (9) for the two regimes.

To simplify the equations, the nondimensional parameters ε, M, and β are introduced where

$$\varepsilon = \frac{V^*}{\omega^*(D^*+L^*)} \ll 1 \; ; \quad M = \frac{V^*}{c^*} \ll 1 \; ; \quad \beta = \frac{\omega^*(D^*+L^*)}{V^*} \ll 1$$

Note that $M<<\varepsilon$ or β. The simplified equations corresponding to the linear regime are

$$\frac{M^2}{\epsilon^2}\frac{\partial p}{\partial t} + \frac{\partial}{\partial r}(r^2 u) + \frac{M^2}{\epsilon}\frac{\partial}{\partial r}(\rho u r^2) = 0 \tag{10}$$

$$\frac{\partial u}{\partial t} + \epsilon u \frac{\partial u}{\partial r} + \left(1 - \frac{M^2}{\epsilon} p\right)\frac{\partial p}{\partial r} - \left[\frac{\nu^*}{\omega^*(D^* + L^*)^2}\right]\left[\begin{matrix}\text{VISCOUS} \\ \text{TERMS}\end{matrix}\right] = 0 \tag{11}$$

$$\left(1 - \frac{M^2}{\epsilon} p\right)\frac{\partial p}{\partial \theta} - \left[\frac{2\nu^*}{\omega^*(D^*+L^*)^2}\right]\frac{1}{r}\frac{\partial u}{\partial \theta} = 0 \tag{12}$$

An examination of the various terms in the continuity equation (Eqn. 10) shows that (1) the second term, which represents the divergence of the volume velocity, is of order unity and is by far the largest term, (2) the first term, which is a measure of the compressibility of the fluid, is very much smaller than the second term (recall that $M<<\varepsilon$) and (3) the third term which represents nonlinear effects is the smallest. What is of interest here is that even for the (linear) case of small amplitude sound approaching an orifice, the flow behaves predominately as if it were incompressible.

It may be of value to offer the following more physical interpretation of the incompressible behavior of the sound field in the orifice neighborhood. Ingard and Ising's hot-wire measurements have shown that the amplitude of the acoustic velocity incident to the orifice increases dramatically from a very small value at a distance of about three orifice diameters to a relatively high value at the orifice outlet. Since this increase occurs over a distance very much smaller than the sound wavelength, it must be a hydrodynamic change rather than an acoustic change. To support this, assume that the length scale (D^*+L^*) characterizing the distance over which the incident (acoustic) velocity change occurs is equal to the sound wavelength (λ^*) divided by 2π (recall that time was scaled with $(\omega^*)^{-1}$ rather than the orifice diameter) Setting $(D^*+L^*) = \lambda^*/2\pi$, then $M = \varepsilon$ and from Eqn. (10) the first term is equal to unity. The third term which represents nonlinear propagation effects is of order ε. Thus, the resulting lowest order equations reduce to the classical spherical wave equations as one would expect. We have shown that compressibility became important only when $\omega^*(D^*+L^*) \simeq c^*$. This means that for practical (wall treatment) sized orifices (e.g. 0.15 cm. diameter), frequencies of the order of 30,000 Hz or higher are required before compressibility effects must be included.

For the nonlinear regime, the simplified equations are

$$M^2\beta \frac{\partial p}{\partial t} + \frac{\partial}{\partial r}(r^2 u) + M^2 \frac{\partial}{\partial r}(\rho u r^2) = 0 \tag{13}$$

$$\beta \frac{\partial u}{\partial t} + u \frac{\partial u}{\partial r} + (1 - M^2 p) \frac{\partial p}{\partial r} - \left[\frac{\nu^*}{V^*(D^* + L^*)}\right]\left[\begin{matrix}\text{VISCOUS} \\ \text{TERMS}\end{matrix}\right] = 0 \tag{14}$$

$$(1 - M^2 p) \frac{\partial p}{\partial \theta} - \left[\frac{2\nu^*}{V^*(D^* + L^*)}\right]\left[\frac{1}{r} \frac{\partial u}{\partial \theta}\right] = 0 \tag{15}$$

Comparing Eqn. (13) with Eqn. (10), we note that they are quite similar. For both regimes the flow incident to the orifice is essentially incompressible. Yet, in contrast to the low pressure case, the compressibility term of Eqn. (13) is smaller (by the fraction β) than the nonlinear term. Thus, the normalization for the two regimes reveals an ordering among the various terms that is consistent and, therefore, lends credence to the validity of the model.

2.1.1 Limitations of Approach

There are several restrictions to the proposed model which impose some limitations on its application. First, it is obvious that the flow does not approach the orifice perfectly spherically, but instead probably has a streaklike pattern (i.e., an instantaneous flow pattern) somewhat like the dashed curve shown in Figure 4(b). We recognize that the instantaneous flow incident to the orifice is only approximately spherical--deviations from a truly spherical flow are required in order to permit the flow to enter the orifice in an axial manner. The spherical flow field is singular at the virtual origin r = o. To avoid this singularity, the spherical flow field is truncated at a hemispherical surface of radius $r^* = L_o^*$ defined such that at this surface the radial acoustic velocity is equal to the maximum value of the actual acoustic velocity through the orifice.

Second, for all but the lowest sound pressure levels, the solution to the equations of motion are valid only when the sound is approaching the orifice--it is not valid during the other half of the cycle when the sound is moving away from the orifice. This limitation is imposed because it has been observed by Labate and Ingard, and Ingard and Ising and others that even for moderately intense sound fields, the acoustic near field velocity separates at the orifice forming a jet-like outflow. Thus the flow is spherical only when it approaches the orifices except for the case of vanishingly small sound fields where separation does not occur. This case, however, has no practical interest because of the extremely low sound pressures involved and will not be

pursued. The third and final limitation is that the orifice characteristic acoustic velocity $\omega^*(D^*+L^*) << c^*$ to maintain the incompressibility of the near field sound.

2.1.2 Boundary Conditions

There are three boundary conditions that must be satisfied. One is that the (radial) velocity u^* must vanish along the walls $\theta = \pi/2$ (see Figure 4a) due to the viscous no-slip condition. The second is that the acoustic pressure p^* must merge smoothly (asymptotically) into the harmonically oscillating driving pressure incident to the orifice. The third and final boundary condition is that at the hemispherical surface $r^* = L_o^*$, where the spherical inflow is truncated, the acoustic pressure p^* must be equal to the orifice back pressure. The orifice back pressure is always constant and equal to its ambient value (this is strictly true only when the orifice exit velocity is subsonic). The acoustic pressure vanishes at $r^* = L_o^*$, the equivalent orifice exit. To be precise, $p^* = o$ at $r^* = L_o^*$ only when the flow Reynolds number $\omega^*(D^*+L^*)^2/\nu^*$ is sufficiently high that the flow separates at the orifice forming a jet. For extremely low Reynolds numbers, the whole flow field is controlled by viscous forces. In this case it is reasonable to assume that the flow field is spherical and not separated on both sides of the orifice.

Expressed mathematically, the boundary conditions are written

$$u\left(r, \Theta = \pi/2, t\right) = o \tag{16}$$

$$\underset{r \to \infty}{\text{LIMIT}} \; p\left(r, \Theta, t\right) = \cos(t) \tag{17}$$

$$p\left[r = \frac{L_o^*}{(D^*+L^*)}, \Theta, t\right] = o \tag{18}$$

The model further assumes that $10(D^*+L^*) << \lambda^*$ so that changes of sound amplitudes and phase are negligible over this distance.

2.2 Linear Regime

The solution to Eqns. (10), (11), and (12) subject to the boundary conditions defined by Eqns. (16), (17), and (18) describe the behavior of orifices exposed to weak to moderate sound fields. Retaining terms to order ε (since $M << \varepsilon$, the effects of compressibility would only weakly affect orifice impedance and are thus ignored) yields

$$\frac{\partial}{\partial r}\left(r^2 u\right) = 0 \tag{19}$$

$$\frac{\partial u}{\partial t} + \frac{\partial}{\partial r}\left(p + \varepsilon \frac{1}{2} u^2\right) - \frac{1}{Re}\left(\begin{matrix}\text{VISCOUS}\\ \text{TERMS}\end{matrix}\right) = 0 \tag{20}$$

$$\frac{\partial p}{\partial \theta} - \frac{2}{Re}\,\frac{1}{r}\,\frac{\partial u}{\partial \theta} = 0 \tag{21}$$

where $Re = \omega^*(D^*+L^*)^2/\nu^*$ is the orifice characteristic Reynolds number. Equation (19), representing the conservation of mass, shows clearly that the flow oscillates through the orifice in an imcompressible (and unsteady) manner.

Much can be learned about the behavior of orifices by carefully examining Eqn. (20). To begin with, assume both $\varepsilon = 0$ and $\nu = 0$ and further that both u and p are harmonically driven so that $u(r,t) = e^{it}\,\tilde{u}(r)$ and $p(r,t) = e^{it}\,\tilde{p}(r)$. Under these circumstances it is clear that u is ninety degrees out of phase with p and that the orifice impedance is reactive only (which it should be if the fluid is frictionless). Now allow the fluid to be real (i.e., viscous). For most practical applications, the orifice characteristic Reynolds number is such that a laminar boundary layer forms along the walls containing the orifice as sketched in Figure 4(b) (assuming typical values of f=1000Hz, (D^*+L^*)=0.15cm, then $Re \simeq 10^3$ which is assumed to be in the laminar Reynolds number range). Thus the resistive losses due to viscosity should be small and hence orifice resistance should be very much less than reactance. Now consider finite values of ε. From Eqn. (20), it is clear that the loss of the fluid kinetic energy $\varepsilon\,\rho u^2/2$ is in phase with the pressure (i.e., resistive) and increases with increasing u. In summary, at very low values of sound pressure, orifice reactance is very much larger than resistance; with increasing sound levels, the resistance should increase because of jet kinetic energy-type resistive losses. This is in complete agreement with the measurements of Ingard and Ising and Thurston et. al. (see Figure 5).

The formal solution to Eqns. (10), (11), and (12) consist of expanding u and p in powers of ε

$$u(r,\theta,t) = u_0(r,\theta,t) + \varepsilon\, u_1(r,\theta,t) + \cdots \tag{22}$$

$$p(r,\theta,t) = p_0(r,\theta,t) + \epsilon\, p_1(r,\theta,t) + \cdots \tag{23}$$

Substituting Eqns. (21a) and (21b) into Eqns. (10), (11) and (12) yields to order ϵ^0 and ϵ

$$\frac{\partial}{\partial r}\left(r^2 u_0\right) = 0 \tag{24}$$

$$\frac{\partial u_0}{\partial t} + \frac{\partial p_0}{\partial r} - \frac{\nu^*}{\omega^*(D^*+L^*)^2}\left[\frac{1}{r^2}\frac{\partial}{\partial r}\left(r^2\frac{\partial u_0}{\partial r}\right) - \frac{2u_0}{r^2} + \frac{1}{r^2\sin\theta}\frac{\partial}{\partial\theta}\left(\sin\theta\frac{\partial u_0}{\partial\theta}\right)\right] = 0 \tag{25}$$

$$\frac{\partial p_0}{\partial\theta} - \frac{2\nu^*}{\omega^*(D^*+L^*)^2}\frac{1}{r}\frac{\partial u_0}{\partial\theta} = 0 \tag{26}$$

and

$$\frac{\partial}{\partial r}\left(r^2 u_1\right) = 0 \tag{27}$$

$$\frac{\partial u_1}{\partial t} + \frac{\partial p_1}{\partial r} + u_0\frac{\partial u_0}{\partial r} - \frac{\nu^*}{\omega^*(D^*+L^*)^2}\left[\text{VISCOUS TERMS}\right] = 0 \tag{28}$$

$$\frac{\partial p_1}{\partial\theta} - \frac{2\nu^*}{\omega^*(D^*+L^*)^2}\frac{1}{r}\frac{\partial u_1}{\partial\theta} = 0 \tag{29}$$

The solution to the above equations must satisfy the boundary conditions specified by Eqns. (16), (17), and (18). The usual procedure in seeking perturbation solutions is to force the lowest-ordered terms to satisfy the boundary conditions with the higher-ordered terms set equal to zero. Thus the appropriate non-dimensionalized boundary conditions are

and

$$u_o(r,\Theta=\pi/2,t)=0 \tag{30}$$

$$\underset{r\to\infty}{\text{LIMIT}}\ p_o(r,\Theta,t)=\cos(t) \tag{31}$$

$$p_o\left[r=\frac{L_o^*}{(D^*+L^*)},\Theta,t\right]=0 \tag{32}$$

and

$$u_1(r,\Theta=\pi/2,t)=0 \tag{33}$$

$$\underset{r\to\infty}{\text{LIMIT}}\ p_1(r,\Theta,t)=0 \tag{34}$$

$$p_1\left[r=\frac{L_o^*}{(D^*+L^*)},\Theta,t\right]=0 \tag{35}$$

2.2.1 Lowest Order Solution

The solution to Eqns. (24), (25), and (26) subject to the boundary conditions given by Eqns. (16) and (17) represent a first approximation to the behavior of the acoustic flow near the orifice. For convenience, the solution will be divided into two parts. In part 1, the effects of viscosity will be ignored. This means that the no-slip boundary condition given by Eqn. (16) will be ignored. The solution to part 2 will include the effects of viscosity.

The solution to Eqn. (24) applies equally to both the inviscid (part 1) and viscous (part 2) solutions and may be immediately integrated to yield

$$u_o(r,\Theta,t)=-\frac{A}{r^2}\,F_o(\Theta,t;Re) \tag{36}$$

where A is an arbitrary constant and F is an unspecified function. The negative sign is included to denote that the velocity is directed radially inwards.

Part I - Inviscid Solution

The equations describing the inviscid behavior of the fluid near the orifice follow from Eqns. (25) and (26) by setting $\nu^*=0$ to yield

$$\frac{\partial u_o}{\partial t} + \frac{\partial p_o}{\partial r} = 0 \tag{37}$$

$$\frac{\partial p_o}{\partial \theta} = 0 \longrightarrow p_o = p_o(r,t) \tag{38}$$

Equation (38) shows that p_o is independent of the azimuthal angle θ. Since p_o is independent of θ, it also follows from Eqn. (37) that u_o is independent of θ and hence from equation (36) that F_o is also independent of θ. Thus, equation (36) becomes

$$u_o(r,t) = -\frac{A}{r^2} F_o(t) \tag{39}$$

Substituting Eqn. (39) into Eqn. (37) yields

$$\frac{\partial}{\partial r}\left[p_o + \frac{A}{r}\frac{dF_o}{dt}\right] = 0$$

which integrates to

$$p_o(r,t) + \frac{A}{r}\frac{dF_o}{dt} = f_o(t) \tag{40}$$

where f(t) is an arbitrary function of time. From the boundary condition given by Eqn. (17), f(t) = cost and Eqn. (40) may be written

$$p_o(r,t) = \cos(t) - \frac{A}{r}\frac{dF_o}{dt} \tag{41}$$

According to our model, the radial inflow accelerates as it approaches the virtual source, hence it must at some radial distance

reach a magnitude at which it is equal to the magnitude of the maximum orifice outlet velocity. It follows since the outlet flow is subsonic that the outlet pressure must be equal to the ambient background pressure. Thus the acoustic perturbation at the orifice outlet must vanish which means that

$$P_o\left[r = \frac{L_o^*}{(D^*+L^*)}, t\right] = 0 \longrightarrow A = L_o^*/(D^*+L^*) \tag{42}$$

Since the acoustic velocity has been normalized to unity at the orifice outlet, we see from Eqns. (39) and (42) that A = r = 1. Thus, the velocity and the pressure written in complex notation for convenience are

$$u_o(r,t) = -\frac{\sin(t)}{r^2} = \frac{ie^{it}}{r^2} \tag{43}$$

and

$$P_o(r,t) = \left(1-\frac{1}{r}\right)\cos(t) = \left(1-\frac{1}{r}\right)e^{it} \tag{44}$$

Equations (43) and (44) are our desired results. Following Ingard and Ising, we define the orifice impedance as the ratio of the driving pressure far (in terms of the characteristic length (D^*+L^*) from the orifice to the velocity at the orifice outlet. Dividing the pressure $P_o = e^{it}$ far upstream of the orifice by the orifice outlet velocity $u_o(r=1,t) = ie^{it}$ yields for the orifice impedance

$$Z = \frac{P_o(r=\infty,t)}{u_o(r=1,t)} = -i \tag{45}$$

In dimensional terms, the impedance is

$$Z^* = -i\rho^*\omega^*(D^*+L^*) \tag{46}$$

There is no resistance, only a negative reactance, because the fluid has been assumed to be inviscid (in the linear sound regime the only mechanism to dissipate acoustic energy is through the fluid viscosity). The negative sign occurs because the inward travelling sound is negative in a spherical coordinate system. Both the orifice resistance and reactance for the linear and nonlinear regimes will be negative for this reason. The orifice

reactance given by Eqn. (45) agrees exceptionally well with the experimental measurements taken by Ingard and Ising and by Thurston, et. al. which is shown in Figure 5. The reactance derived above is virtually identical with the reactance derived by the slug-mass model (Eqn. 2b), thus showing the equivalence of the two models at low sound pressure levels.

Part 2 - Viscous Solution

At low sound pressure levels, Ingard and Ising's measurements showed that the (linear) resistance of an isolated orifice may be approximated by the empirical expression repeated here as,

$$R^* \cong \sqrt{8\mu^*\rho^*\omega^*}\ (1 + L^*/D^*);\ X^* \cong \rho^*\omega^*(L^* + 0.85\,D^*) \qquad (2)$$

Ingard[4] and Crandall's[10] work led to the derivation of Eqn. (2). They solved for the relationship between the pressure gradient, unsteady velocity, and viscosity in an *infinitely* long cylindrical tube containing an unsteady, viscous, fully-developed one-dimensional flow. Ingard[4] later corrected this to include finite orifice thickness by including as an end correction, the viscous contributions of the side walls containing the orifice. This lead to the development of Eqn. (2). A major deficiency of this approach is that for most practical orifices of interest, the orifice thickness is *small* compared to the orifice diameter rather than very large as the derivation requires. In this sense, the end correction is not a correction at all but represents instead the major part of the losses (i.e., the losses associated with the viscous flow along the side walls containing the orifice) with the losses *inside* the orifice being small.

For orifices where $L^* \ll D^*$, the use of an end correction to account for viscous losses as given by Eqn. (2a) is unnecessary. It follows logically from the proposed model that the viscous losses arise from the boundary layer established by the radial flow moving inwards along the side walls containing the orifice. The importance of viscous effects are characterized by the flow field Reynolds number. If the Reynolds number is large, then viscous effects are important usually within a small region called the boundary-layer region. Conversely, if the Reynolds number is small, viscous effects are important throughout the whole region of interest. Assuming values representative of the orifices used as acoustic liners in present day jet aircraft, that is $(D^*+L^*) \cong 0.15$ CM, $f \cong 10^3$ HZ, $\nu^* \cong 0.15\ \text{CM}^2/\text{SEC}$, then the Reynolds number $R_e \cong 10^3$ which is sufficiently large to model viscous effects using boundary-layer theory.

Boundary-layer theory assumes (1) that viscous effects are important only within a small region, in the present application, adjacent to the side walls containing the orifice, (2) the pressure gradient normal to the wall is negligible, hence the pressure is constant through the boundary layer and its value is derived from inviscid theory and (3) that the velocity at the wall surface is zero and approaches asymptotically at the boundary layer edge its inviscid value. The appropriate boundary-layer equations to be solved are

$$\frac{\partial}{\partial r}\left(r^2 u_o\right) = 0 \tag{47}$$

$$\frac{\partial u_o}{\partial t} + \frac{\partial p_o}{\partial r} - \frac{1}{Re}\left[\frac{1}{r^2}\frac{\partial}{\partial r}\left(r^2\frac{\partial u_o}{\partial r}\right) - \frac{2u_o}{r^2} + \frac{1}{r^2\sin\Theta}\frac{\partial}{\partial\Theta}\left(\sin\Theta\frac{\partial u_o}{\partial\Theta}\right)\right] = 0 \tag{48}$$

$$\frac{\partial p_o}{\partial\Theta} = 0 \tag{49}$$

Equation (48) can be simplified further by introducing the transformation $\zeta = \pi/2 - \Theta$ and observing that since the boundary layer is confined to the immediate neighborhood of the wall where $\Theta \cong \pi/2$ (see Figure 4b), then ζ is very small and we may approximate $\sin\Theta \cong \cos(\zeta) \simeq 1$. Introducing the angle ζ and the above approximation into Eqn. (48) yields

$$\frac{\partial u_o}{\partial t} + \frac{\partial p_o}{\partial r} - \frac{1}{Re}\left[\frac{1}{r^2}\frac{\partial}{\partial r}\left(r^2\frac{\partial u_o}{\partial r}\right) - \frac{2u_o}{r^2} + \frac{1}{r^2}\frac{\partial^2 u_o}{\partial\zeta^2}\right] = 0 \tag{50}$$

Eqn. (47) may be integrated and inserted into Eqn. (50) which, after some algebraic manipulation, yields

$$u_o(r, \zeta, t; Re) = \frac{ie^{it}F_o(\zeta, Re)}{r^2} \tag{51}$$

where we have used complex notation and note explicitly that the function F_o depends both upon the angle ζ and the Reynolds number R_e. From boundary-layer theory and from the no-slip boundary condition, Eqn. (16), $F_o(\zeta, Re)$ must satisfy that

$$F_o(\zeta=0; Re) = 0 \quad \text{and} \quad \underset{\substack{Re\to\infty \\ \zeta>0}}{\text{LIMIT}} F_o(\zeta; Re) = 1 \tag{52}$$

The boundary condition on the function F_o has been selected so that the viscous velocity u approaches asymptotically (with increasing Reynolds number) its inviscid value defined by Eqn. (43). Using Eqn. (44) for the (inviscid) pressure and substituting u_o and p_o into Eqn. (50) yields after some algebra

$$-F_o(\zeta)+1-\frac{i}{Re\, r^2}\frac{d^2}{d\zeta^2}F_o(\zeta;Re)=0 \tag{53}$$

To recover the boundary-layer character of Eqn. (53), we introduce the boundary-layer coordinate η defined by

$$\eta=\sqrt{Re}\; r\,\zeta \tag{54}$$

and set $F_o(\zeta,Re) = F_o(\eta)$. Physically, this means that the velocity is invariant to the transformation defined by Eqn. (47). Substituting Eqn. (54) into Eqn. (53) yields

$$-F_o(\eta)+1-i\frac{d^2F_o(\eta)}{d\eta^2}=0 \tag{55}$$

The solution to Eqn. (55) that satisfies the boundary conditions given by Eqn. (52) is

$$F_o(\eta)=1-e^{\frac{-(1+i)\sqrt{2}}{2}\eta} \tag{56}$$

Substituting Eqn. (56) into Eqn. (51) and solving for the real part yields for the velocity u_o

$$u_o(r,\eta,t)=-\frac{1}{r^2}\left[\sin(t)-e^{-\sqrt{2}\,\eta/2}\sin(t-\sqrt{2}\,\eta/2)\right] \tag{57}$$

The instantaneous velocity distribution (Eqn. 57) is uniform everywhere near the orifice except near the walls $\theta = \pi/2$ where the velocity decreases from its uniform value to zero through a

thin (boundary layer) region of thickness $Re^{-1/2}$. The retarding action of the fluid viscosity acts, for a given driving excitation pressure, to decrease the magnitude of the acoustic velocity pumped through the orifice by an amount related to the displacement thickness δ^* defined as

$$u_o\delta^* = \frac{1}{\sqrt{2Re}} \int_o^\infty \left[u_o(r,t) - u_o(r,\eta,t)\right] d\eta \tag{58}$$

Substituting Eqn. (57) into Eqn. (58) yields

$$u_o\delta^* = -\frac{1}{r^2\sqrt{Re}} \left[\sin(t) - \cos(t)\right] \tag{59}$$

Since $u_0\delta^*$ represents the amount of mass "lost" because of the effects of viscosity, the effective velocity approaching the orifice is

$$u_o(r,t) = u_o(1-\delta^*) = -\frac{\sin(t)}{r^2}\left(1 - \frac{1}{\sqrt{2Re}}\right) - \frac{\cos(t)}{r^2\sqrt{2Re}} \tag{60}$$

At r = 1 (the effective orifice outlet), the velocity is, written in complex notation,

$$u_o(1,t) = e^{it}\left[i\left(1 - \frac{1}{\sqrt{2Re}}\right) - \frac{1}{\sqrt{2Re}}\right] \tag{61}$$

Dividing the pressure $p = e^{it}$ incident to the orifice by the velocity u_o given by Eqn. (61) yields for the orifice impedance

$$(-Z) \cong \frac{1}{\sqrt{2Re}}\left[1 + \sqrt{\frac{2}{Re}}\right] + i\left[1 + \frac{1}{\sqrt{2Re}}\right] \tag{62}$$

Resolving Z into its real (resistance) and imaginary (reactance) parts yields

$$\left[-R\right] \cong \frac{1}{\sqrt{2\,Re}}\left[1+\sqrt{\frac{2}{Re}}\right] \tag{63}$$

and

$$\left[-X\right] \cong 1+\frac{1}{\sqrt{2\,Re}} \tag{64}$$

Written in dimensional terms, the impedance is

$$\left[-Z^*\right] \cong \left[\sqrt{\frac{\rho^*\omega^*\mu^*}{2}}+\frac{\mu^*}{(D^*+L^*)}\right]+i\left[\rho^*\omega^*(D^*+L^*)+\sqrt{\frac{\rho^*\mu^*\omega^*}{2}}\right] \tag{65}$$

Equation (65) is of interest because it shows the behavior of orifice resistance as $\omega^*\to 0$, namely $(-R)\to\mu^*/(D^*+L^*)$. Thus, we see that the effects of viscosity are to generate a resistance given by Eqn. (63) and to perturb the inviscid reactance (Eqn. 45) by the small (constant) amount given by Eqn. (64).

The orifice (linear) resistance was derived using the concept of a boundary-layer displacement thickness which may be interpreted physically as a loss of mass flow along the walls containing the orifice due to the retarding effects of viscosity. The derivation demonstrates clearly that the proposed spherical model, based on fluid mechanical concepts, is the proper way to understand the acoustic behavior of orifices. In contrast, Ingard and Ising interpret their (linear) orifice resistance data (for their orifice $L^*<<D^*$--see Figure 1) in terms of a "viscous end correction". But the fundamental derivation of this "end correction" by Rayleigh and others assumed that to first order the orifice thickness was infinitely long (i.e., $L^*>>D^*$). Their derivation assumed that the oscillatory motion of the fluid contained within the orifice thickness was equivalent to a solid body oscillation. To force agreement between theory and measurements an "end correction" was added. To apply this model to predict the resistance of their orifices where $L^*<D^*$ is clearly unsatisfactory although the empirical formula (Eqn. 2) is in agreement with experimental findings. This approach, however, breaks down when it is extended to predict orifice nonlinear resistance. The solid body oscillation approach is clearly incompatible with the observed nonlinear jetting or "breaking away" of the fluid from the orifice. In contrast, the model presented herein does not have these deficiencies, but instead includes, in a straight forward manner, the important effects of viscosity and jetting on the orifice resistance *and reactance*.

The predicted linear orifice resistance (Eqn. 63) differs from the empirical prediction (Eqn. 2a) by the factor (2). Applying both equations to the orifice viscous resistance data measured by Ingard and Ising (summarized in Figure 2--here $L^*<<D^*$), it would

appear, at first glance, that Eqn. (2a) was more accurate. We shall show that this may not be true because nonlinear effects will be shown below to be important even at the low orifice velocities.

2.2.2 First-Order Solution

The differential equations (27), (28), and (29) represent nonlinear corrections (of order $\varepsilon u_0 \partial u_0/\partial r$) to the lower ordered linear solution. To simplify the analysis, only the inviscid correction will be sought. Thus, $\nu^* = 0$ and the equations describing the first order corrections become

$$\frac{\partial}{\partial r}\left(r^2 u_1\right) = 0 \tag{66}$$

$$\frac{\partial u_1}{\partial t} + \frac{\partial p_1}{\partial r} + u_0 \frac{\partial u_0}{\partial r} = 0 \tag{67}$$

$$\frac{\partial p_1}{\partial \theta} = 0 \longrightarrow p_1 = p_1(r,t) \tag{68}$$

Equation (67), in its present form, is misleading. By rewriting it in the form

$$\frac{\partial u_1}{\partial t} + \frac{\partial}{\partial r}\left(p_1 + \frac{1}{2} u_0^2\right) = 0,$$

it is clear that the term $1/2 u_0^2$ is in phase with the pressure p_1. Since it is always positive, it must be replaced with $1/2\ u_0|u_0|$ if it is to be in phase with the harmonically fluctuating pressure p_1. This restriction is based mostly on Ingard and Ising's hot-wire measurements which showed that u_0 fluctuated harmonically (at least along the orifice center line). An alternate explanation is that the model is valid only during the half-cycle during which the acoustic velocity is approaching the orifice; to account for the other half, the coordinate system must be mathematically "switched" to the *other* side of the orifice. While the linear terms account for this automatically, the non-linear term $1/2 u_0^2$ does not. It follows from this discussion that the correct momentum equation is

$$\frac{\partial u_1}{\partial t} + \frac{\partial}{\partial r}\left(p_1 + \frac{1}{2}|u_0|u_0\right) = 0 \tag{67a}$$

Integrating Eqn. (66) yields for the first-order velocity

$$u_1(r,t) = -F_1(t)/r^2 \tag{69}$$

where $F_1(t)$ is an arbitrary function of time.

Substituting Eqn. (69) into Eqn. (67a) and integrating with respect to r yields

$$\frac{1}{r}\frac{dF_1}{dt} + p_1 + \frac{1}{2}|u_o|u_o = f_1(t) \tag{70}$$

where $f_1(t)$ is also an arbitrary function of time and u_o is given by Eqn. (43). From the boundary contition specified by Eqn. (33)

$$\underset{r\to\infty}{\text{Limit}}\; p_1(r,t) = 0 \quad \rightarrow f_1(t) = 0 \tag{71}$$

Thus, Eqn. (70) reduces to

$$\frac{1}{r}\frac{dF_1}{dt} = -\left(p_1 + \frac{1}{2}|u_o|u_o\right) \tag{72}$$

For application to nonlinear flow, the model assumes that at the radial location r = 1, the flow $u_o + \varepsilon u_1$ is accelerated to its maximum value and the pressure $p_o + \varepsilon p_1$ (providing the maximum velocity $u_o + \varepsilon u_1$ is subsonic) is equal to the ambient background pressure. Thus, the acoustic perturbation p_1 must vanish when the velocity is a maximum and we write at r = 1

$$p_1(r=1,t) = 0 \tag{73}$$

Substituting Eqn. (73) into (72) yields at r = 1

$$\frac{dF_1}{dt} = -\frac{1}{2}|u_o|u_o = +\frac{1}{2}|\sin(t)|\sin(t) \tag{74}$$

The integration of Eqn. (74) is split into two parts, one corresponding to t>o and the other to t<o. Thus, Eqn. (74) integrates to

$$F_1(t) = \begin{cases} -\frac{1}{4}\left[t - \sin(t)\cos(t)\right], & t<0 \\ +\frac{1}{4}\left[t - \sin(t)\cos(t)\right], & t>0 \end{cases} \tag{75}$$

where the constant of integration has been ignored.

Since we are interested primarily in predicting orifice impedance, only the fundamental harmonic component of Eqn. (75) is of interest. Using Fourier analysis, and noting that $F_1(t)$ is an even function, it is straight-forward to show that

$$a_1 = \frac{2}{\pi}\int_0^{\pi} F_1(t)\cos(t)\,dt = 4/3\,\pi \tag{76}$$

and hence that

$$F_1(t) \cong \frac{4}{3\pi}\cos(t) \tag{77}$$

Combining Eqns. (69) and (77) yields for the nonlinear velocity u_1,

$$u_1(r,t) \cong -\frac{4}{3\pi r^2}\cos(t) \tag{78}$$

The orifice velocity, including both viscous and nonlinear contributions, follows (written in complex notation) by combining Eqns. (60) and (70) to yield,

$$u(r,t) \cong \frac{ie^{it}}{r^2}\left(1-\frac{1}{\sqrt{2Re}}\right) - \frac{e^{it}}{r^2}\left(\frac{4\varepsilon}{3\pi} + \frac{1}{\sqrt{2Re}}\right) \tag{79}$$

Again, defining orifice impedance as the ratio of the driving acoustic pressure to the orifice velocity, it follows that

$$(-Z) \cong \frac{1}{\left(\frac{4\varepsilon}{3\pi} + \frac{1}{\sqrt{2Re}}\right) - i\left(1-\frac{1}{\sqrt{2Re}}\right)} \tag{80}$$

The real and imaginary parts of Z are

$$-R \simeq \left(\frac{1}{\sqrt{2Re}} + \frac{1}{Re}\right) + \frac{4\varepsilon}{3\pi}\left(1 + \sqrt{\frac{2}{Re}} - \frac{1}{Re}\right) \tag{81}$$

$$(-X) \cong 1 + \frac{1}{\sqrt{2Re}}\left(1-\frac{8\varepsilon}{3\pi}\right) \tag{82}$$

Both Ingard and Ising and Thurston et. al presented their orifice impedance data in terms of the ratio of the incident

driving acoustic pressure to the orifice *inlet* velocity. The definition of impedance used in this model is based on the maximum orifice velocity rather than the inlet velocity. Before the orifice resistance and reactance defined by Eqns. (81) and (82) can be compared with the experimental data of Ingard and Ising and Thurston, et. al, these differences must be resolved. Significant differences occur between the orifice inlet and maximum (vena contracta) velocities only for the part of the orifice velocity that is in-phase (resistive) with the incident driving pressures. Orifice flows that are in-phase with pressure can be characterized as quasi-steady and the concept of a discharge coefficient C_D (suitably time-averaged) can be introduced to connect the orifice inlet velocity V_i to its maximum value V (at the vena contracta) where

$$V_i = C_D V \tag{83}$$

In steady-state flows through orifices, the discharge coefficient is used because it conveniently determines the mass flow through the orifices for a given driving pressure. In most applications, the characteristic flow Reynolds number is sufficiently high (above about 1000) that the discharge coefficient is constant. The solution of the nonlinear acoustic velocity u_1 shows that (1) it is in phase with the driving pressure p_0 (see Eqn. 78), (2) it is quadratically related to the u_0 (see Eqns. 44 and 67) and (3) it is independent of viscosity (this corresponds to flows of infinite Reynolds numbers). It is clear that u_1 is quasi-steady and inviscid and falls within the category of a Bernouilli-type of flow. Thus, to connect the model results with experimental data, Eqn. (83) is used to replace V by V_i in the definition of the perturbation parameter ε rewritten as

$$\varepsilon = \frac{V_i^*}{C_D \omega^* (D^* + L^*)} \tag{84}$$

Substituting Eqns. (83) and (84) into Eqns. (81) and (82) yields the final form of the resistance and reactance.

$$-R \cong \left(\frac{1}{\sqrt{2Re}} + \frac{1}{Re}\right) + \frac{4}{3\pi C_D}\left[\frac{V_i^*}{\omega^*(D^*+L^*)}\right]\left(1+\sqrt{\frac{2}{Re}} + \frac{1}{Re}\right) \tag{85}$$

and

$$(-X) \cong 1 + \frac{1}{\sqrt{2Re}}\left\{1 - \frac{8}{3\pi C_D}\left[\frac{V_i^*}{\omega^*(D^*+L^*)}\right]\right\} \tag{86}$$

Transforming Eqns. (85) and (86) to dimensional terms

$$(-R^*) \cong \underbrace{\sqrt{\frac{\rho^*\mu^*\omega^*}{2}}\left(1+\sqrt{\frac{2}{Re}}\right)}_{\text{viscous loss}} + \underbrace{\frac{4\rho^* V_i^*}{3\pi C_D}\left(1+\sqrt{\frac{2}{Re}}-\frac{1}{Re}\right)}_{\text{jet loss}} \tag{87}$$

and

$$(-X^*) \cong \underbrace{\rho^*\omega^*(D^*+L^*)}_{\substack{\text{oscillating slug mass} \\ \text{model recovered}}} + \sqrt{\frac{\rho^*\omega^*\mu^*}{2}}\left[1-\frac{8V_i^*}{3\pi C_D \omega^*(D^*+L^*)}\right] \tag{88}$$

The negative signs occur in Eqns. (87) and (88) because the sound field is incoming. The orifice resistance described by Eqn. (87) consists primarily of the sum of two terms, one representing a nonlinear Bernouilli-type of jetting effect and the other a viscous dissipation loss effect. The orifice reactance, described by Eqn. (88), is also the sum of two terms, one representing an oscillating mass flow term and the other a higher-ordered combined viscous and nonlinear (Bernouilli) term. Equation (88) shows the nature of the cross-coupling between the nonlinear Bernouilli effect and orifice reactance. The effect is to weakly decrease orifice reactance. The effect is weak because the derivation requires that $V_i^* << \omega(D^*+L^*)$ which restricts the magnitude of the jetting effect. The existence of a weak reduction in orifice reactance has been observed experimentally over a wide range of test conditions including the experiments by Ingard and Ising with air (Fig. 2) and Thurston, et. al. with water (Fig. 3). A direct comparison between the reactance predicted by Eqn. (88) and the experiments by Ingard and Ising and Thurston, et. al is shown in Fig. 5. The comparison is excellent.

Since $V_i^*/\omega^*(D^*+L^*) \ll 1$, it follows that $|R| << |X|$ and that the orifice impedance $Z = \sqrt{R^2+X^2} \cong X$ is virtually constant. Although the nonlinear Bernouilli term only weakly affects the reactance and hence the impedance, it can dominate the viscous resistance term in Eqn. (85) providing that

$$\frac{3\pi C_D}{4\sqrt{2Re}} \ll \frac{V_i^*}{\omega^*(D^*+L^*)} \ll 1 \tag{89}$$

Thus an interesting behavior or embedding exists wherein the resistance is dominated by nonlinear (jet) losses of the kind described by Ingard and Ising but the impedance is dominated by an almost

constant reactance - hence the impedance is, to first order, constant.

To verify the usefulness of Eqn. (87), it should be compared with the experimental data of Ingard and Thurston. Unfortunately, the behavior of the discharge coefficient C_D at these low velocities is not available. As an indirect means of verifying its usefulness, Eqn. (87) will be forced to agree with Ingard's and Thurston's measurements by computing the required values of C_D. The results of this force fit are shown in Fig. 6 in terms of the required values of C_D. The shape of the required C_D curve is similar to the measured C_D data shown in Melling's paper[11] which shows the effect of Reynolds number. The similarity between these curves despite their difference in diameter (D*), thickness to diameter ratio (L*/D*), and the fact that one represents a force fit to a.c. resistance data and the other d.c. test data is encouraging. To verify the usefulness of the model and hence Eqn. (87), detailed a.c. tests of the dependence of C_D to geometry and Reynolds number are required.

2.3 Nonlinear Regime

The basic equations governing the behavior of intense sound fields near orifices were derived in Section 2.1 above and are defined by Eqns. (13), (14), and (15). In the nonlinear regime, the characteristic orifice Reynolds number, $Re = V^*(D^*+L^*)/\nu^*$ is independent of the frequency in contrast to the Reynolds number characterizing the linear regime, $Re = \omega^*(D^*+L^*)^2/\nu^*$. Since the Reynolds number is fairly large in the nonlinear regime (typical jet engine linear values are $V^* = 50$ m/sec, $(D^*+L^*) = 1.5\times10^{-3}$m, $\nu^* = 0.15\times10^{-4}$m^2/sec to yield $Re \simeq 5000$), the contribution of viscous terms to the orifice impedance will be ignored.

Retaining terms to order β and ignoring viscous terms, Eqns. (13), (14), and (15) simplify to

$$\frac{\partial}{\partial r}\left(r^2 u\right) = 0 \tag{90}$$

$$\beta\frac{\partial u}{\partial t} + u\frac{\partial u}{\partial r} + \frac{\partial p}{\partial r} = 0 \tag{91}$$

$$\frac{\partial p}{\partial \theta} = 0 \quad \rightarrow \quad p = p(r,t) \tag{92}$$

The velocity follows immediately from Eqn. (90) to be

$$u(r,t) = -F(t)/r^2 \tag{93}$$

where F(t) is an arbitrary function of time. Substituting Eqn. (93) into Eqn. (91) and integrating with respect to radial distance (r) yields

$$(\beta/r)\frac{dF}{dt} + p + F^2/2r^4 = g(t) \tag{94}$$

where g(t) is yet another arbitrary function of time. Since viscosity is ignored, the no-slip boundary condition specified by Eqn. (16) does not have to be satisfied. The pressure, however, must satisfy the boundary contitions specified by Eqns. (17) and (18). Applying the boundary condition specified by Eqn. (17) to Eqn. (94), it is clear that g(t) = cos(t). Applying the boundary condition specified by Eqn. (18), p(r = 1, t) = o, yields the following equation at r = 1

$$\beta \frac{dF}{dt} + \frac{1}{2}F^2 = \cos(t) \tag{95}$$

The solution to Eqn. (95) describes the *time behavior* of the vena contracta velocity (i.e., the maximum velocity of the jet exiting the orifice). Equation (95) is a nonlinear differential equation of the Riccati type. Since, to our knowledge, there are no known analytical solutions to Eqn. (95), an approximate solution is sought sufficiently accurate to elucidate its physical interpretation. Since $\beta << 1$, the contribution of the unsteady term is relatively unimportant; the orifice behaves in an essentially quasi-steady manner.

The usual procedure to solve Eqn. (95) in an approximate way is to expand the function F in powers of β and to solve, say, for the first two functions F_0, F_1 defined below as

$$F(t,\beta) \simeq F_o(t) + \beta F_1(t) + \cdots \tag{96}$$

This kind of approach, however, breaks down and the solutions to F_0 and F_1 become singular for values of $t = (2n - 1)\pi/2$, $n = 0, 1, 2....$ To illustrate this singular behavior, the solution to Eqn. (96), assuming that $\beta = 0$, is

$$F_o(t) = \sqrt{2\cos(t)} \tag{97}$$

The derivative of (F) in Eqn. (97) is of order unity everywhere except near $t = (2n-1)\pi/2$ where it becomes singular. Physically, the flow oscillates through the orifice with period $2\pi\omega^{-1}$ and near $t = (2n - 1)\pi/2$ the function F_0 is both small and rapidly decelerating (or accelerating). Thus, near $t = (2n - 1)\pi/2$ the assumption that $|\beta\, dF/dt| \ll |1/2\, F^2|$ is incorrect and both terms in Eqn. (95) must be retained.

The singular behavior of F(t, β) is analogous to the singular behavior of boundary-layer type flows wherein large changes to the flow tangential to a surface occur within a small region. A successful procedure to remove such singularities is to use the method of singular perturbation theory. The details of the derivation that follows are described in the Appendix. To start with, Eqn. (95) is transformed to the boundary layer form

$$-\frac{df}{d\xi} + f^2 \cong \xi - \delta^{4/3}\left(\frac{1}{6}\xi^3\right) + O\left(\delta^{8/3}\right) \tag{98}$$

where

$$F(t;\beta) = \sqrt{2}\,\delta^{1/3} f(\xi;\delta)\,; \quad \xi = (\pi/2 - t)/\delta^{2/3}\,; \quad \delta = \sqrt{2}\,\beta \tag{99}$$

To solve Eqn. (98), the boundary-layer type function f is expanded as follows

$$f(\xi,\delta) = f_0(\xi) + \delta^{4/3} f_1(\xi) + O\left(\delta^{8/3}\right) \tag{100}$$

Substituting Eqn. (100) into Eqn. (98) and collecting the coefficients of δ^0 and $\delta^{4/3}$ yields

$$-\frac{df_0}{d\xi} + f_0^2 = \xi \tag{101}$$

$$-\frac{df_1}{d\xi} + 2 f_0 f_1 = -\frac{1}{6}\xi^3 \tag{102}$$

2.3.1 Solution to Order β^0

Equation (101) is the well-known Riccati equation whose solution can be expressed in terms of the Airy function Ai(ξ) as

$$f_0(\xi) = -\dot{A}_i(\xi)/A_i(\xi) \tag{103}$$

where $(\dot{})$ denotes the operator $d/d\xi$. A plot of the functions $f_0(\xi)$ and $f_0(\xi)/\sqrt{\xi}$ are shown in Figure 7. It is evident that the function $f_0(\xi)$ has the correct asymptotic behavior to properly match to the inner behavior of $F(t;\beta)$ (the details of the matching of the inner and outer functions are given in the Appendix). Defining the thickness of the inner region (ξ_{in}) as the value of ξ_{in} where $f_0(\xi_{in}) \cong 0.99\sqrt{\xi_{in}}$, then from Figure 7, $\xi_{in} \simeq 5$. Thus, to first order the solution to Eqn. (95) is

$$F(t;\beta) \cong \begin{cases} \sqrt{2\cos(t)}\ , & 0 \le t \le \pi/2 - 2^{1/3}(5)\beta^{2/3} \\ \sqrt{2}\,\beta^{1/3} f_o\left[\dfrac{\pi/2 - t}{2^{1/3}\beta^{2/3}}\right]\ , & \dfrac{\pi}{2} - 2^{1/3}(5)\beta^{2/3} \le t \le \pi/2 \end{cases} \tag{104}$$

It is convenient to rewrite Eqn. (104) in the following form

$$F(t) \cong \sqrt{2\cos(t)} + 2^{2/3}\beta^{1/3}\,\Delta f_o\left[\xi(t)\right] \tag{105}$$

where $\Delta f(t)$ is defined in Figure 8. Substituting Eqn. (105) into Eqn. (93), the radial velocity approaching the orifice is approximately

$$u(r,t) = -F(t)/r^2 \cong -1/r^2\left\{\sqrt{2\cos(t)} + 2^{2/3}\beta^{1/3}\Delta f_o\left[\xi(t)\right]\right\} \tag{106}$$

The harmonic component of Eqn. (106) is determined approximately by Fourier analyzing the resulting expression yielding

$$u(r,t) \cong -\frac{1.57\cos(t) - 1.62\,\beta\sin(t)}{r^2} \tag{107}$$

2.3.2 Solution to Order $\beta^{4/3}$

The solution to Eqn. (102) represents the first-order correction to $f_0(\xi)$. The homogeneous solution to Eqn. (102) is

$$f_1^h(\xi) = A\,e^{2\int_0^{\xi} f_o(x)\,dx} \tag{108}$$

where A is an arbitrary constant of integration. The particular solution is

$$f_1^p(\xi) = \frac{1}{6}\, e^{2\int_0^{\xi} f_0(x)\,dx} \int_0^{\xi} e^{-2\int_0^{y} f_0(x)\,dx}\, y^3\, dy \tag{109}$$

The general solution to Eqn. (102) is

$$f_1(\xi) = f_1^h(\xi) + f_1^p(\xi) \tag{110}$$

The only way to match the outer solution of Eqn. (110) to the inner behavior of $F(t;\beta)$ is to set $A = 0$. Thus, to order $\beta^{4/3}$, the solution to Eqn. (95) is

$$F(t;\beta) \cong \begin{cases} \sqrt{2\cos(t)}\ , \quad 0 \le t \le \frac{\pi}{2} - 5(2^{1/3})\beta^{2/3} \\ 2^{2/3}\beta^{1/3}\left\{f_0\left[\xi(t)\right] + 2^{2/3}\beta^{4/3} f_1\left[\xi(t)\right]\right\} \\ \qquad\qquad \pi/2 - 5(2^{1/3})\beta^{2/3} \le t \le \pi/2 \end{cases} \tag{111}$$

A plot of the functions $f_1(\xi)$ and its asymptotic behavior $-1/12\ \xi^{5/2}$ is shown in Figure 9. In a manner similar to that used in the derivation of the approximate solution given by Eqn (104), a solution to order $\beta^{4/3}$ of Eqn. (95) is

$$F(t;\beta) \cong \sqrt{2\cos(t)} + 2^{2/3}\beta^{1/3}\,\Delta f_0\left[\xi(t)\right] + 2^{4/3}\beta^{5/3}\Delta f_1\left[\xi(t)\right] \tag{112}$$

where the function $\Delta f_1[\,\xi(t)]$ is defined in Fig. 10. The harmonic component of Eqn. (112) is determined by Fourier analysis to yield

$$F(t;\beta) \cong -1.57\cos(t) - (1.62\beta + 4.04\beta^{7/3})\sin(t) \tag{113}$$

Thus the harmonic component of the radial inflow u_1 written in complex notation for convenience, is approximately

$$u_1(r,t) \cong -\frac{\left[1.57\, e^{it} + i e^{it}(1.62\beta + 4.04\beta^{7/3})\right]}{r^2} \tag{114}$$

Following Ingard and Ising, we define orifice impedance as the ratio of acoustic pressure far from the orifice to the orifice inlet velocity V_i^*. As described earlier in Section 2.2.2, the relationship between the orifice inlet velocity and the orifice maximum velocity V^* (vena contracta velocity) is defined as

$$V_i^* = C_D V^* \tag{115}$$

where C_D is the time-averaged discharge coefficient. Equation (115) is valid only for the part of the velocity that is in phase with the driving pressure. Replacing $u_1(r,t)$ at $r = 1$ with $C_D^{-1} u_i$ in Eqn. (114) yields the following estimate of the orifice outlet velocity u_i written in complex notation

$$u_1 = -1.57 C_D e^{it} + i\left(1.62\beta + 4.04\beta^{7/3}\right) e^{it} \tag{116}$$

Using Eqn. (116), the orifice impedance is

$$(-Z) = \frac{e^{it}}{1.57 C_D e^{it} - i\left(1.62\beta + 4.04\beta^{7/3}\right) e^{it}} \tag{117}$$

The orifice resistance and reactance follows from Eqn. (117) to be approximately

$$(-R) \cong \frac{0.64}{C_D}\left[1 - \left(\frac{1.03\beta}{C_D}\right)^2\right] \tag{118}$$

and

$$(-X) \cong \frac{0.66\beta}{C_D^2}\left[1 + 2.48\beta^{4/3}\right]\left[1 - \left(\frac{1.03\beta}{C_D}\right)^2\right] \tag{119}$$

In dimensional terms, the resistance and reactance are

$$(-R^*) \simeq \frac{0.64\rho^* V_i^*}{C_D^2}\left[1 - \frac{1.06 C_D^2 \omega^{*2}(L^* + D^*)^2}{(V_i^*)^2}\right] \tag{120}$$

and

$$\left[-X^*\right] \cong \frac{0.66\rho^*\omega^*(D^*+L^*)}{C_D^2}\left\{1+2.48\left[\frac{C_D\omega^*(D^*+L^*)}{V_i^*}\right]^{4/3}\right\}\left[1-\frac{1.06\,C_D^2\omega^*(D^*+L^*)}{V_i^{*2}}\right] \quad (121)$$

To compare the predicted orifice behavior with the data by Ingard and Ising and Thurston et.al, Eqns. (120) and (121) are nondimensionalized by the quantity $\rho^*\omega^*(D^*+L^*)$ to yield the final form

$$\left[\frac{-R^*}{\rho^*\omega^*(D^*+L^*)}\right] \cong \frac{0.64}{C_D^2}\left[\frac{V_i^*}{\omega^*(D^*+L^*)}\right]\left[1-1.06\left(\frac{C_D\omega^*(L^*+D^*)}{V_i^*}\right)^2\right] \quad (122)$$

and

$$\left[\frac{-X^*}{\rho^*\omega^*(D^*+L^*)}\right] \cong \frac{0.66}{C_D^2}\left\{1+2.48\left[\frac{C_D\omega^*(D^*+L^*)}{V_i^*}\right]^{4/3}\right\}\left\{1-1.06\left[\frac{C_D\omega^*(D^*+L^*)}{V_i^*}\right]^2\right\} \quad (123)$$

Equations (122) and (123) must be interpreted with caution because of two key assumptions made in their derivation. First, the solution is valid only when the sound field is approaching the orifice it is not valid during the other half of the cycle when the sound is moving away from the orifice. Second, the orifice reactance was derived only near $t = \pi/2$ (where the flow direction changes) - it was assumed to be zero at $t = 0$. It is clear from Ingard and Ising's measurements, that the phase shift between the driving pressure and the orifice velocity is constant for a constant driving sound pressure and frequency. Thus a reasonable correction to Eqn. 123 would be to reduce its value to one-half under the assumption that by forcing the reactance to be zero at $t = 0$, the reactance at $t = \pi/2$ is likely to be twice its true value. This is possible even with the first assumption because Ingard and Ising have shown that the orifice inflow is symmetrical during each half-cycle. Accordingly, Eqn. (123) is reduced by one-half to

$$\left[\frac{-X^*}{\rho^*\omega^*(D^*+L^*)}\right] \cong \frac{0.33}{C_D^2}\left\{1+2.48\left[\frac{C_D\omega^*(D^*+L^*)}{V_i^*}\right]^{4/3}\right\}\left\{1-1.06\left[\frac{C_D\omega^*(D^*+L^*)}{V_i^*}\right]^2\right\} \quad (124)$$

Equations (122) and (124) show that orifice resistance and reactance are coupled through C_D the discharge coefficient. To verify the utility of the model, the orifice resistance and reactance

measured by Ingard and Ising for air (D = 7mm, f = 150Hz) and by Thurston, et. al for water (D = 3mm, f = 22Hz) are compared with the predicted values determined by Eqns. (122) and (124). Choosing $C_D = 0.80$ the predicted values compare remarkably well (particularly the shape) with the measurements for both very different test conditions (for air and for water) as shown in Fig. 5.

The model shows clearly that at high sound pressure levels where $V_i^* >> \omega^*(D^*+L^*)$, orifices behave in a predominately quasi-steady manner in agreement with the experimental findings of Zorumski and Parrott[12]. Both orifice resistance and reactance are shown to be related to a time-averaged discharge coefficient. The quasi-linear behavior of the orifice is now clear. Over most of the cycle the orifice reactance term $|\beta \partial u/\partial t| << |u \partial u/\partial x|$ except near the turning points where $t = (2n-1)\pi/2$. The analysis shows that reactance is important only when $\pi/2-(5)(2^{1/3})(\beta^{2/3}) < t < \pi/2$ or about $(5)(2^{1/3})(\beta^{2/3})/\pi/2$ of a cycle. Physically, this means that the slight phase shift between the driving pressure and the orifice velocity is unimportant over most of cycle but becomes important when the orifice velocity is sufficiently low (of the order $\beta^{1/3}$) that the slight phase shift dominates and the orifice flow direction reverses.

3. SUMMARY OF RESULTS

The results of this model extends significantly our understanding of the acoustic behavior of orifices, particularly reactance. The model has direct and important application to the connection between the optimum wall impedance required for maximum sound attenuation and the wall construction having this desired impedance.

The results of this study show the following:

. The acoustic flow in the immediate neighborhood of the orifice (i.e., the near field) can be modelled as a locally spherical flow. Within this near field, the flow is, to a first approximation, unsteady and incompressible. This is true regardless of the intensity of the incident sound pressure field. Thus the behavior of orifices are hydrodynamic rather than acoustic.

. The behavior of orifices can be roughly divided into three regimes depending upon the value of the ratio $V_i^*/\omega^*(D^*+L^*)$ where V_i is the magnitude of the orifice inlet velocity, ω^* is the sound radian frequency, and (D^*+L^*) is the orifice diameter and thickness respectively. When $V_i^*/\omega^*(D^*+L^*) << 1$, orifice reactance is much larger than resistance and the orifice impedance is constant, independent of the incident sound pressure (the so-called "linear" regime). When $V_i^*/\omega^*(D^*+L^*) >> 1$, orifice resistance is much larger than reactance and the orifice behaves in a quasi-steady manner, (the so-called "nonlinear" regime). When $V_i^*/\omega^*(D^*+L^*) = 0(1)$, orifice resistance is approximately equal to reactance.

The parameter $V_i^*/\omega^*(D^*+L^*)$ can be directly related to the incident sound field. In the linear regime, $V_i^* = P^*/\rho^*\omega^*(D^*+L^*)$ where ρ^* is the fluid mean density and P^* is the amplitude of the incident sound field. Thus, in the linear regime, the ratio

$V_i^*/\omega^*(D^*+L^*) = P^*/\rho^*[\omega^*(D^*+L^*)]^2 << 1$. In the nonlinear regime, $V_i^* = [C_D P^*/\rho^*]^{1/2}$ where C_D is an orifice time-averaged discharge coefficient. Thus, in the nonlinear regime, the ratio $V_i^*/\omega^*(D^*+L) = (C_D P^*/\rho^*)^{1/2}/\omega^*(D^*+L^*) >> 1$ (to be consistent with the parameter used above for the linear regime, one could use, since $C_D \simeq 0(1)$, $P^*/\rho^*[\omega^*(D^*+L^*)]^2 >> 1$ to identify the nonlinear regime). The intermediate regime where orifice resistance and reactance are roughly equal can be identified when $P^*/\rho^*[\omega^*(D^*+L^*)]^2 \simeq 1$.

. For $P^*/\rho^*[\omega^*(D^*+L^*)]^2 << 1$, corresponding to a reactance dominated orifice impedance, orifice resistance consists of two terms, one a viscous term related to the boundary layer displacement along the walls containing the orifice and the other a jetting type term related to the flow nonlinearity. With the exception of extremely low sound fields, the nonlinear resistance dominates the viscous resistance; its behavior is expressed in terms of a time-average discharge coefficient. Comparison between the model and data shows that the discharge coefficient is a function of the ratio $P^*/\rho^*[\omega^*(D^*+L^*)]^2$. Despite the existence of the nonlinear resistance term, the orifice impedance is virtually constant because $|X| >> |R|$.

. For $P^*/\rho[\omega^*(D^*+L^*)]^2 >> 1$, corresponding to a resistance dominated orifice impedance, the orifice behaves in a quasi-steady manner in agreement with the experimental findings of Zorumski and Parrott[12]. Both the orifice resistance and reactance are shown to be related to a time-averaged discharge coefficient.

. The results of the model have been compared with the orifice impedance measurements by Ingard and Ising in *air* and by Thurston et. al in *water* and the agreement between prediction and measurement is excellent.

APPENDIX

SUPPORTING ANALYSIS

To simplify the amount of analysis presented in Section 2, many of the supporting or intermediate steps were omitted. For those interested, they are described below.

Equations (7), (8) (9)

Assuming spherical symmetry, the flow field incident to the orifice is

$$r^{*2}\frac{\partial \rho^*}{\partial t} + \rho^*\frac{\partial}{\partial r^*}(r^{*2}u^*) + r^{*2}u^*\frac{\partial \rho^*}{\partial r^*} = 0 \qquad \text{(A-1)}$$

$$\frac{\partial u^*}{\partial t^*} + u^*\frac{\partial u^*}{\partial r^*} + \frac{1}{\rho^*}\frac{\partial p^*}{\partial r^*} - \nu^*\left[\frac{1}{r^{*2}}\frac{\partial}{\partial r^*}\left(r^{*2}\frac{\partial u^*}{\partial r^*}\right)\right.$$

$$\left. - \frac{2u^*}{r^*} + \frac{1}{r^{*2}\sin\theta}\frac{\partial}{\partial \theta}\left(\sin\theta\frac{\partial u^*}{\partial \theta}\right)\right] = 0 \qquad \text{(A-2)}$$

$$\frac{\partial p^*}{\partial \theta} - 2\frac{\mu^*}{r^*}\frac{\partial u^*}{\partial \theta} = 0 \qquad \text{(A-3)}$$

Assuming that the flow field incident to the orifice consists of a steady-state part and an oscillating part, then we can write

$$\begin{aligned} p^*(r^*,\theta,t^*) &= \bar{p}^* + p^{*\prime}(r^*,\theta,t^*) \\ \rho^*(r^*,\theta,t^*) &= \bar{\rho}^* + \rho^{*\prime}(r^*,\theta,t^*) \\ u^*(r^*,\theta,t^*) &= \qquad u^{*\prime}(r^*,\theta,t^*) \end{aligned} \qquad \text{(A-4)}$$

Substituting Eqn. (A-4) into Eqns. (A-1), (A-2), and (A-3) and subtracting out the steady-state terms yields

$$r^{*2}\frac{\partial \rho^{*\prime}}{\partial t^*} + \bar{\rho}^*\frac{\partial}{\partial r^*}(r^{*2}u^{*\prime}) + \frac{\partial}{\partial r^*}(\rho^{*\prime}u^{*\prime}r^{*2}) = 0 \qquad \text{(A-5)}$$

$$\frac{\partial u^{*\prime}}{\partial t^*} + u^{*\prime}\frac{\partial u^{*\prime}}{\partial r^*} + \frac{1}{\bar{\rho}^*}\left(1-\rho^{*\prime}/\bar{\rho}^*\right)\frac{\partial p^{*\prime}}{\partial r^*}$$

$$-\bar{\nu}^*\left[\frac{1}{r^{*2}}\frac{\partial}{\partial r^*}\left(r^{*2}\frac{\partial u^{*\prime}}{\partial r^*}\right) - 2\frac{u^{*\prime}}{r^{*2}} + \frac{1}{r^{*2}\sin\theta}\frac{\partial}{\partial\theta}\left(\sin\theta\frac{\partial u^{*\prime}}{\partial\theta}\right)\right] = 0 \quad \text{(A-6)}$$

$$\left(1-\rho^{*\prime}/\bar{\rho}^*\right)\frac{\partial p^{*\prime}}{\partial\theta} - \frac{2\bar{\mu}^*}{r^*}\frac{\partial u^{*\prime}}{\partial\theta} = 0 \quad \text{(A-7)}$$

To be precise $\bar{\mu}^*$ and $\bar{\nu}^*$ should be replaced with the expressions $\bar{\mu}^* + \mu^{*1}$ and $\bar{\nu}^* + \nu^{*1}$ but this refinement will be ignored. Equations (7), (8) and (9) of Section 2 follow immediately upon substituting into Eqns. (A-5), (A-6) and (A-7), the non-dimensional variables r, t, u, p, ρ from Eqn. (6) and the characteristic values of P^*, ρ^*, V^*, (D^*+L^*) and $(\omega^*)^{-1}$ described in Section 2.1.

Solution to Eqn. (116)

Introducing the transformations $F(t;\beta) = \sqrt{2}\,G(t;\delta)$, $\delta = \sqrt{2}\beta$ into Eqn. (95) results in a simplified equation

$$\delta\frac{dG}{dt} + G^2 = \cos(t) \quad \text{(A-8)}$$

Since we are interested in the behavior of Eqn. (A-8) in the neighborhood of $t = \pi/2$ (where it is singular - see discussion following Eqn. (97), we introduce the transformations

$$G(t;\delta) = G(\tau;\delta)\,, \quad \tau = \pi/2 - t \quad \text{(A-9)}$$

into Eqn. (A-8) resulting in

$$-\delta\frac{dG}{d\tau} + G^2 = \sin(\tau) \quad \text{(A-10)}$$

We are interested in the behavior of Eqn. (A-10) near $\tau = 0$. Anticipating a boundary-layer type behavior near $\tau = 0$, the solution to Eqn. (A-10) is divided into two regions, one called the "outer" region where

$$\left| \delta \frac{dG}{d\tau} \right| << \left| G^2 \right| \tag{A-11}$$

and the other the "inner" region where

$$\left| \delta \frac{dG}{d\tau} \right| \sim O \left| G^2 \right| \tag{A-12}$$

An approximate solution to Eqn. (A-11) for $\delta = 0$ and τ small is

$$G(\tau; \delta = 0) \simeq \sqrt{\sin(\tau)} \simeq \tau^{1/2} - \frac{1}{12} \tau^{5/2} + O(\tau^{9/2}) \tag{A-13}$$

In the terminology of singular perturbation theory, Eqn. (A-13) is called the outer solution. Note that $dG/d\tau$ is infinite (singular) at $\tau = 0$ ($t = \pi/2$). To remove the singularity, the inner variable ξ and inner function $f(\xi;\delta)$ are introduced

$$G(\xi; \delta) = \delta^b f(\xi; \delta), \quad \xi = \tau / \delta^a \tag{A-14}$$

where a and b are constants that are determined below.

The idea here is to transform both the dependent and independent variables of Eqn. (A-10) in such a way that both terms on the LHS are of equal importance. The transformation is valid only within a small region near $\tau = 0$ (or $t = \pi/2$). The boundary condition governing the transformed inner solution are determined by proper matching for large values of ξ to the outer solution given by Eqn. (A-13). To be precise, proper matching occurs when the inner behavior of the outer solutions matches asymptotically with the outer behavior of the inner solution. To demonstrate this, Eqn. (A-13) is rewritten with τ replaced by $\delta^a \xi$,

$$G(\delta^a \xi; \delta = 0) \simeq \delta^{a/2} \xi^{1/2} - \frac{1}{12} \delta^{5a/2} \xi^{5/2} + O(\delta^{9a/2}) \tag{A-15}$$

The transformation defined by Eqn. (A-14) must asymptotically (for ξ large) match Eqn. (A-15). Substituting Eqn. (A-14) into Eqn. (A-10) and expanding for small δ, t fixed, yields

$$-\delta^{(1+b-a)}\frac{df}{d\xi}+\delta^{2b}f^2=\sin\left(\delta^a\xi\right)\cong\delta^a\xi-\frac{1}{6}\delta^{3a}\xi^3+O\left(\delta^{5a}\right) \tag{A-16}$$

A meaningful solution to Eqn. (A-16) follows upon setting

$$1+b-a=2b=a \tag{A-17}$$

yielding

$$a=2/3\ ,\ b=1/3 \tag{A-18}$$

Thus

$$G(\tau;\delta)=\delta^{1/3}f(\xi;\delta)\ ,\ \xi=\tau/\delta^{2/3} \tag{A-19}$$

Substituting Eqn. (A-18) into Eqn. (A-16) yields

$$-\frac{df}{d\xi}+f^2\cong\xi-\delta^{4/3}\left(\frac{1}{6}\xi^3\right)+O\left(\delta^{8/3}\right) \tag{A-20}$$

To solve Eqn. (A-20), expand f as follows

$$f(\xi,\delta)\cong f_o(\xi)+\delta^{4/3}f_1(\xi)+\delta^{8/3}f_2(\xi)+O(\delta^{12/3}) \tag{A-21}$$

where the function $f_o(\xi)$ and $f_1(\xi)$ must have the following asymptotic behavior to properly match the inner and outer solutions.

$$\underset{\xi\to\infty}{\text{LIMIT}}\ f_o(\xi)=\xi^{1/2} \tag{A-22}$$

and

$$\underset{\xi\to\infty}{\text{LIMIT}}\ f_1(\xi)=-\frac{1}{12}\xi^{5/2} \tag{A-23}$$

Substituting Eqn. (A-21) into Eqn. (A-20) and collecting the coefficients of δ° and δ' yields

$$-\frac{df_\circ}{d\xi} + f_\circ^2 = \xi \tag{A-24}$$

and

$$-\frac{df_1}{d\xi} + 2 f_\circ f_1 = -\frac{1}{6}\xi^3 \tag{A-25}$$

REFERENCES

1. Morse, P. M., "The transmission of Sound Inside Pipes", J. Acoust. Soc. Am., Vol. 11, 1939, p. 205.

2. Cremer, L. Akust. Beih. 2,249-263, 1953, (translated by G. B. de Montolvo of McDonnell-Douglas Aircraft Co.)

3. Rice, E. J., "Propagation of Waves in an Acoustically Lined Duct with a Mean Flow", NASA SP-207, 345-355, Basic Aerodynamic Research Conference, 1969.

4. U. Ingard, "On the Theory and Design of Acoustic Resonators", Journ. Acoust. Soc. Am., Vol 25, 1953, 1037-1062.

5. Lord Rayleigh: Theory of Sound - 1945 (re-issue) New York, Dover Publications.

6. Sirignano, William A., "Non Linearita dei Risonatori di Helmholtz", Aerotecnica Missili E. Spazio N. 4-1972.

7. Zinn, B. T., "A Theoretical Study of Nonlinear Damping by Helmholtz Resonators", Preprint No. 69-481, AIAA 5th Propulsion Specialists Meeting, June, 1966.

8. Ingard, Uno and Ising, Harmut, "Acoustic Non-linearity of an Orifice", J. Acoust. Soc. Am., Vol. 42, No. 1, 1967, 6-17.

9. Thurston, G. B., Hargrove, Jr., L.E., and Cook, W. D., "Nonlinear Properties of Circular Orifices", Jour. Acoust. Soc. Am., Vol. 29, No. 9, 1957, 992-1001.

10. Crandall, S., Theory of Sound, Van Nostrand Co., 1927.

11. Melling, T. H., "The Acoustic Impedance of Perforates at Medium and High Sound Pressure Levels", Jour. Sound Vib. Vol. 29, pt. 1, 1973, 1-65.

12. Zorumski, W. E. and Parrott, Tony L., "Nonlinear Acoustic Theory for Rigid Porous Materials" NASA TND-6196, June 1971.

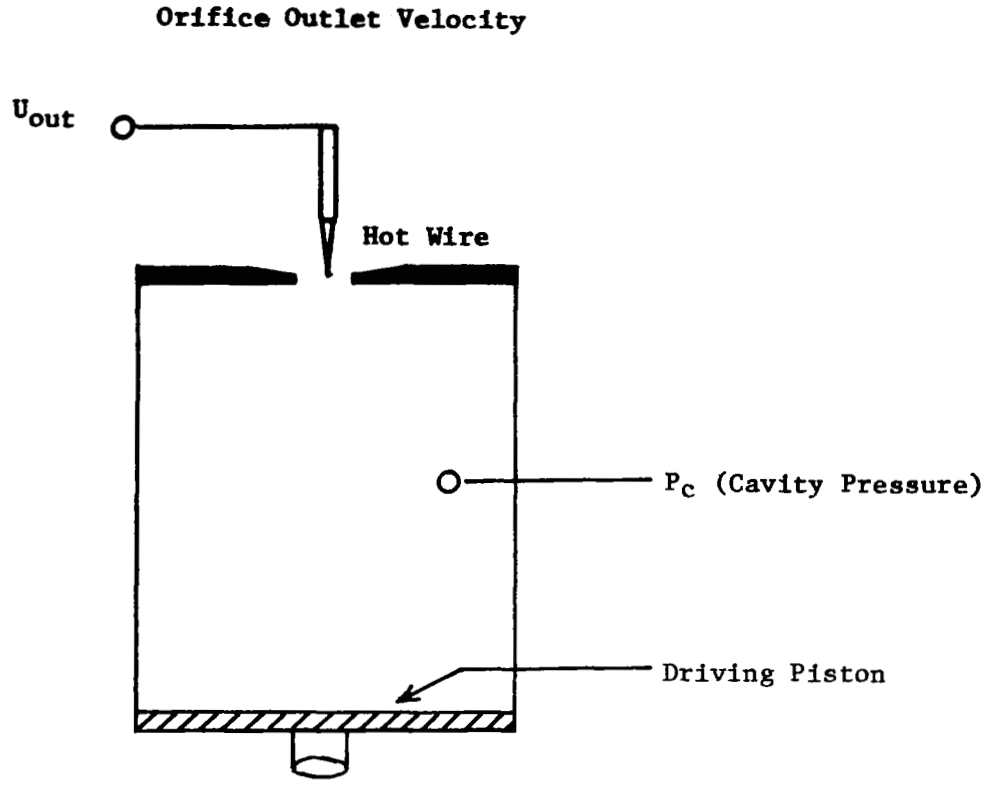

FIGURE 1. INGARD AND ISING EXPERIMENTAL ARRANGEMENT

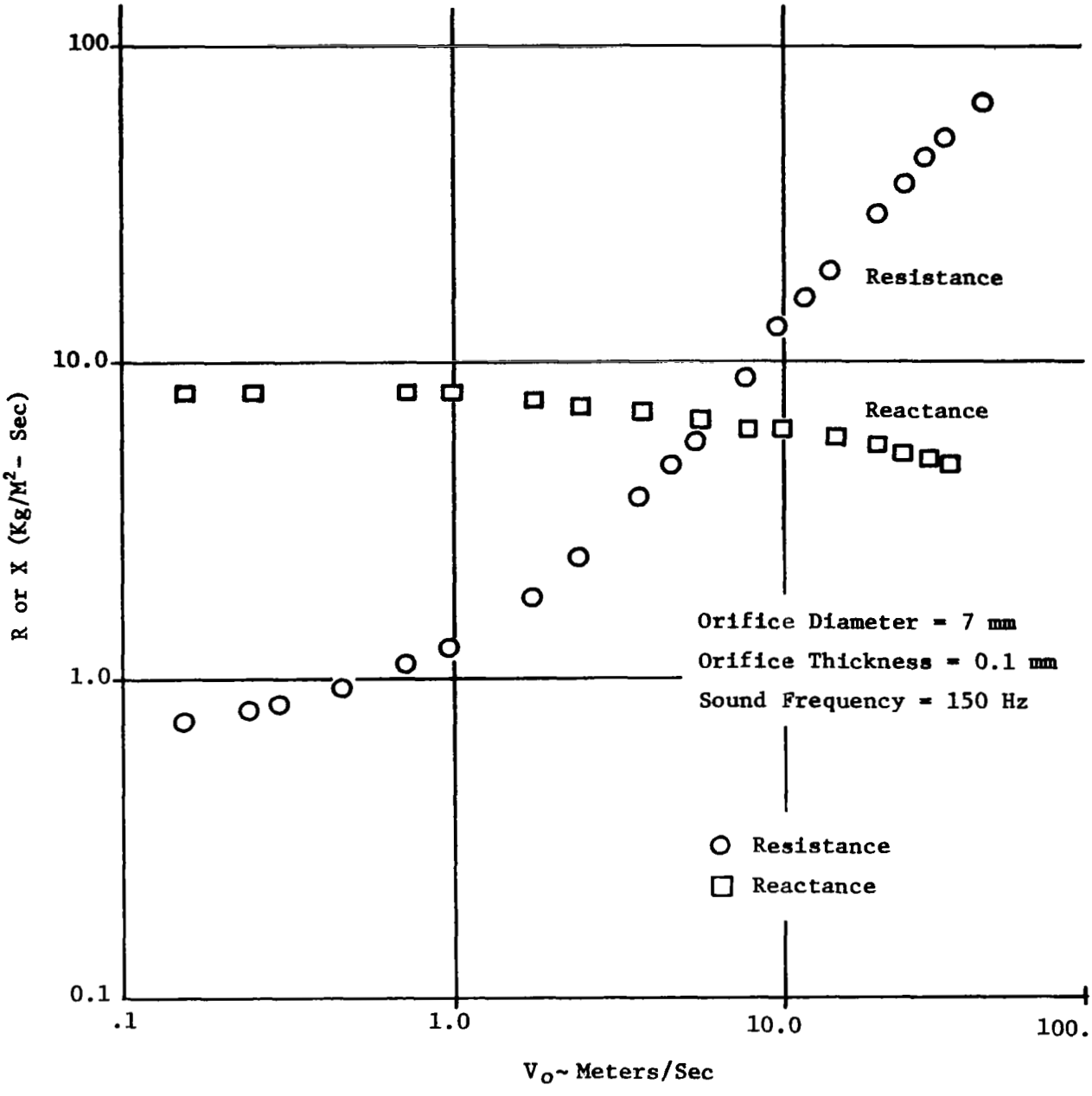

FIGURE 2. INGARD AND ISING'S MEASUREMENTS OF ORIFICE IMPEDANCE

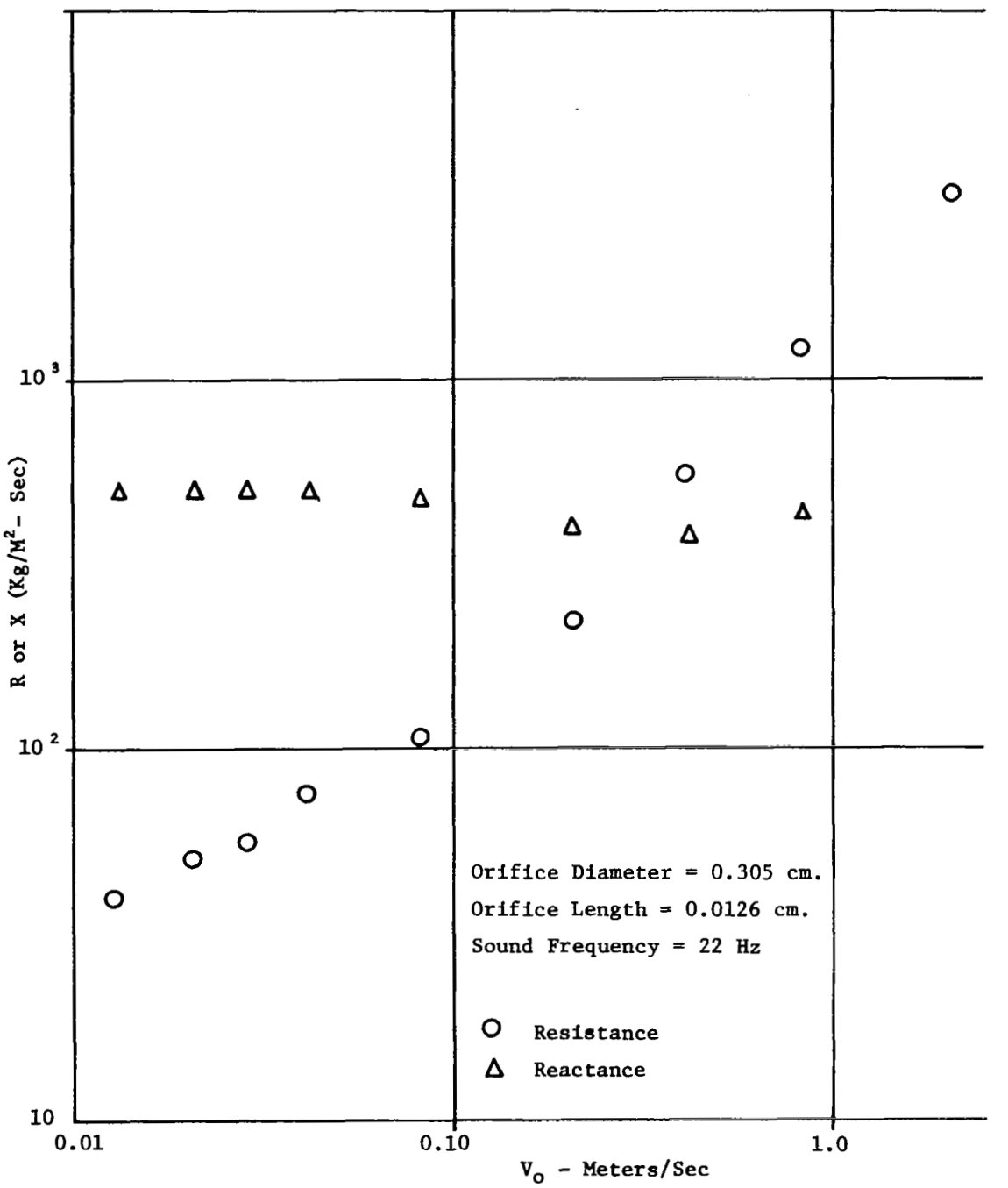

FIGURE 3. THURSTON'S ET. AL. MEASUREMENTS OF ORIFICE IMPEDANCE

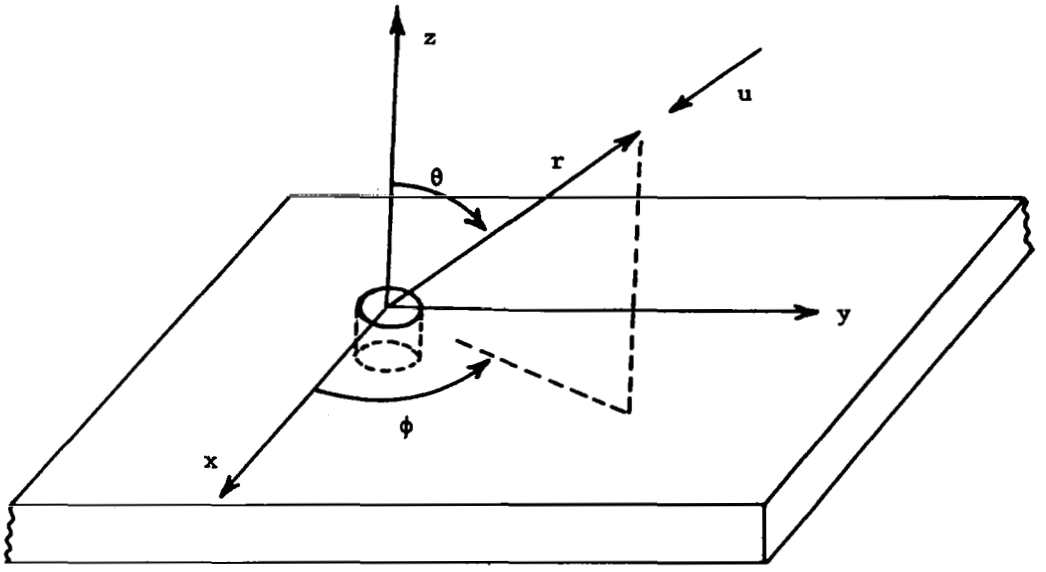

FIGURE 4A. COORDINATE SYSTEM USED IN ORIFICE MODEL

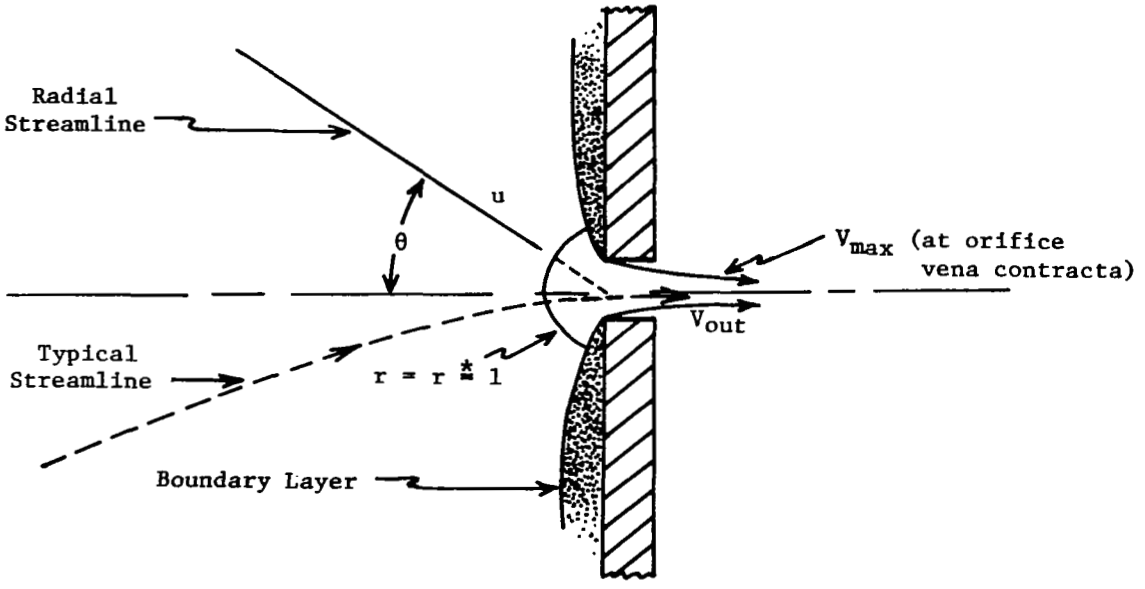

FIGURE 4B. SKETCH OF FLOW FIELD NEAR ORIFICE

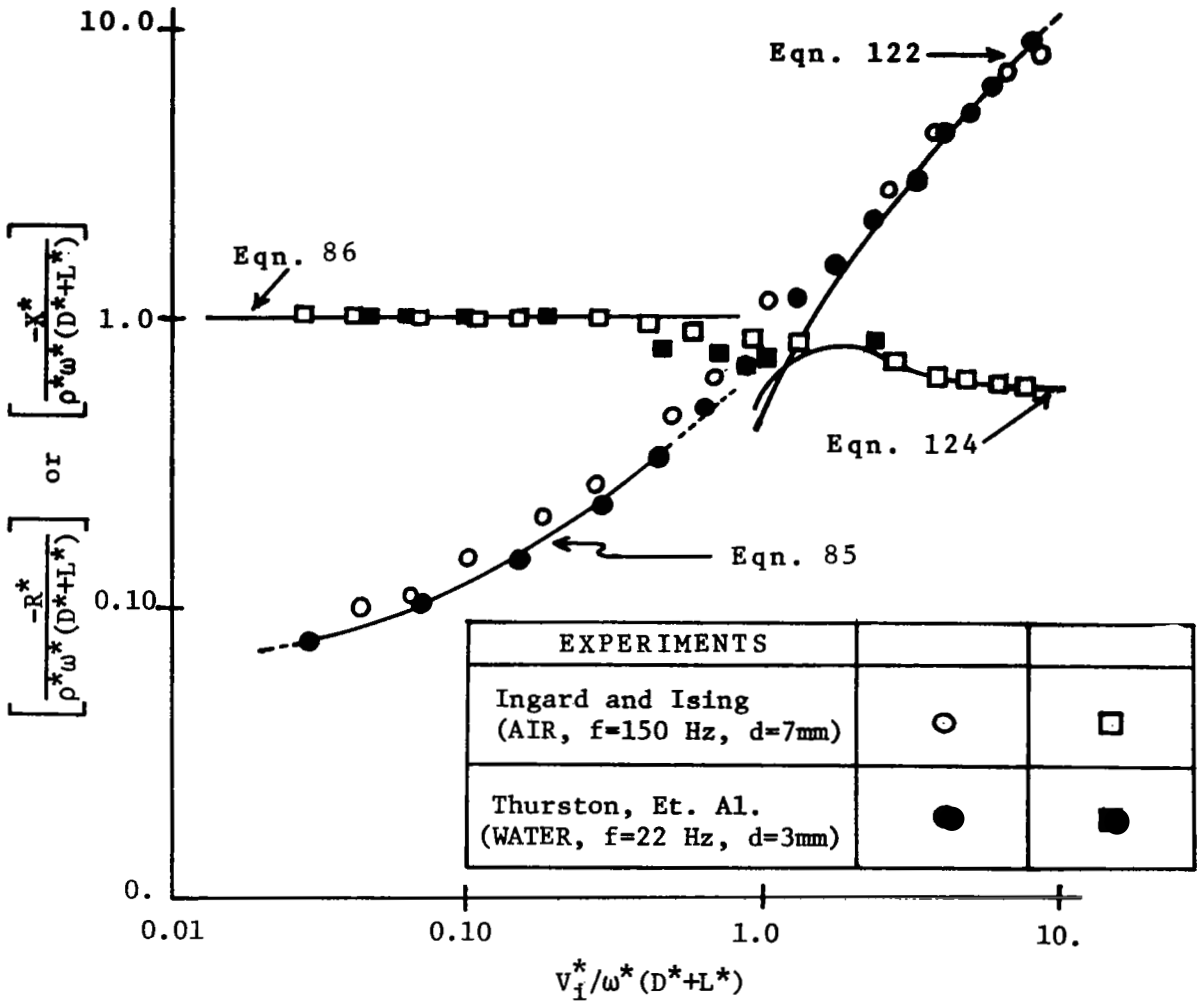

FIGURE 5. COMPARISON BETWEEN PREDICTED AND MEASURED ORIFICE IMPEDANCE

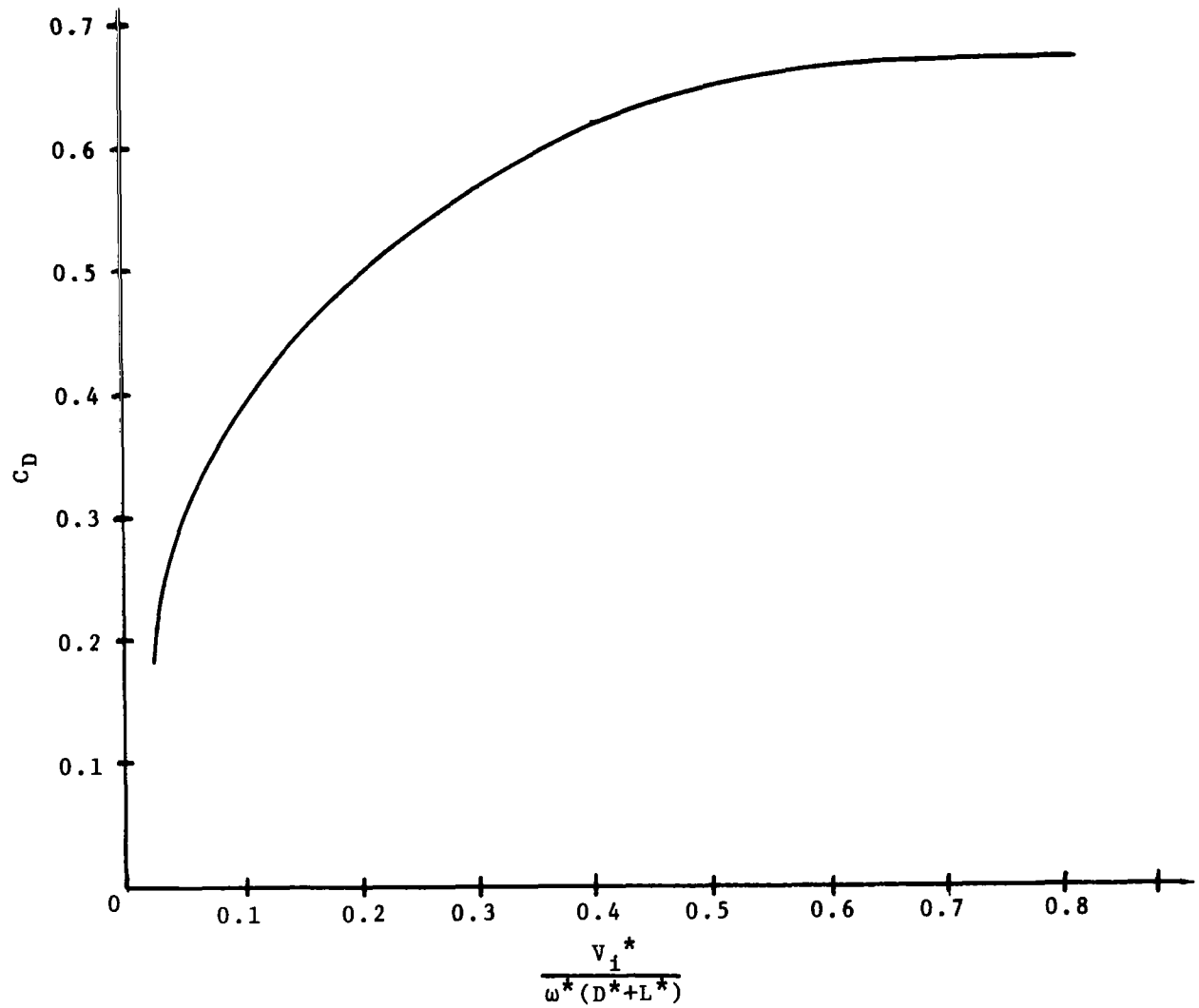

FIGURE 6. VALUE OF C_D REQUIRED TO FORCE EQUATION (85) TO MATCH DATA

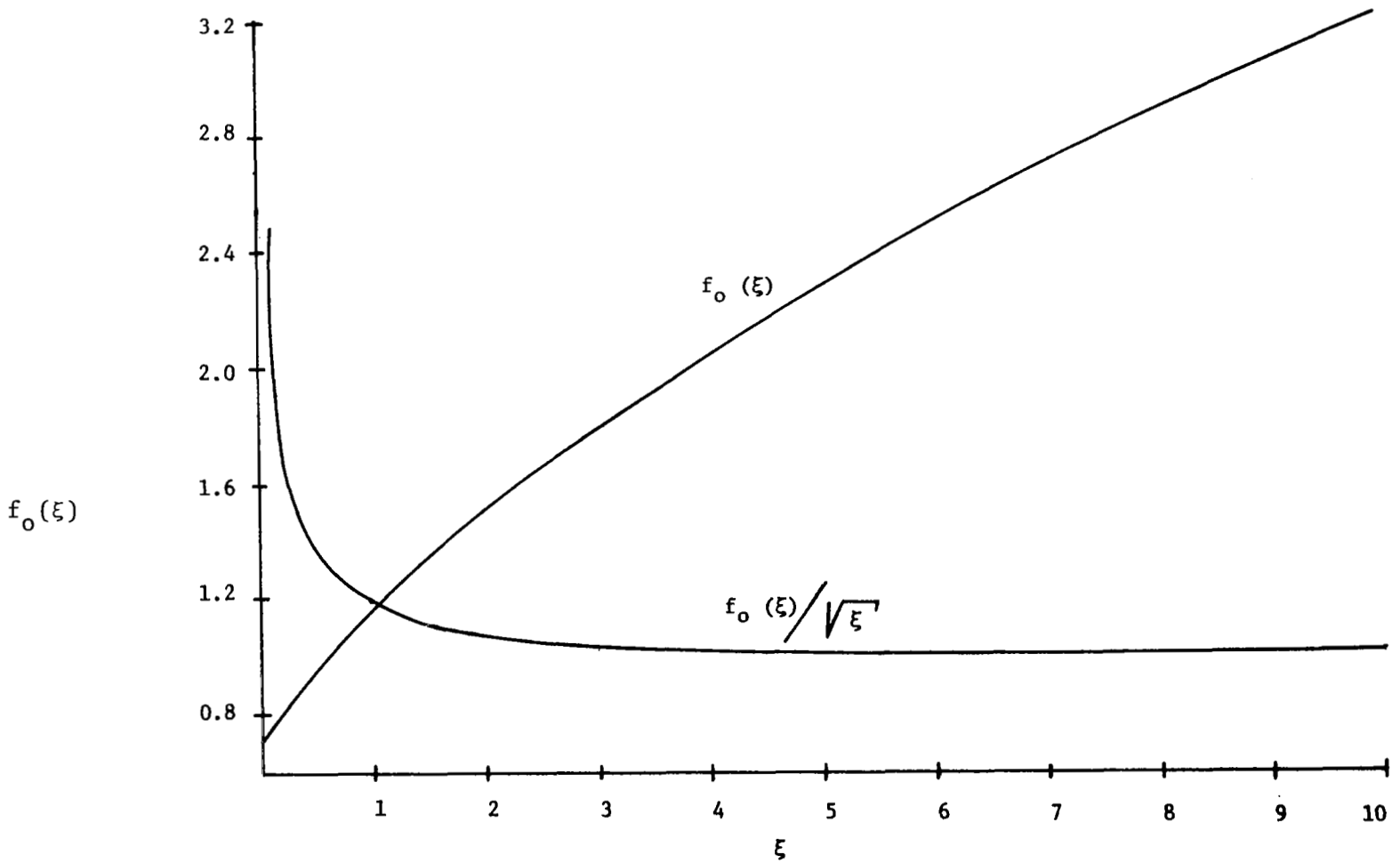

FIGURE 7. SOLUTION OF THE FUNCTION $f_o(\xi)$

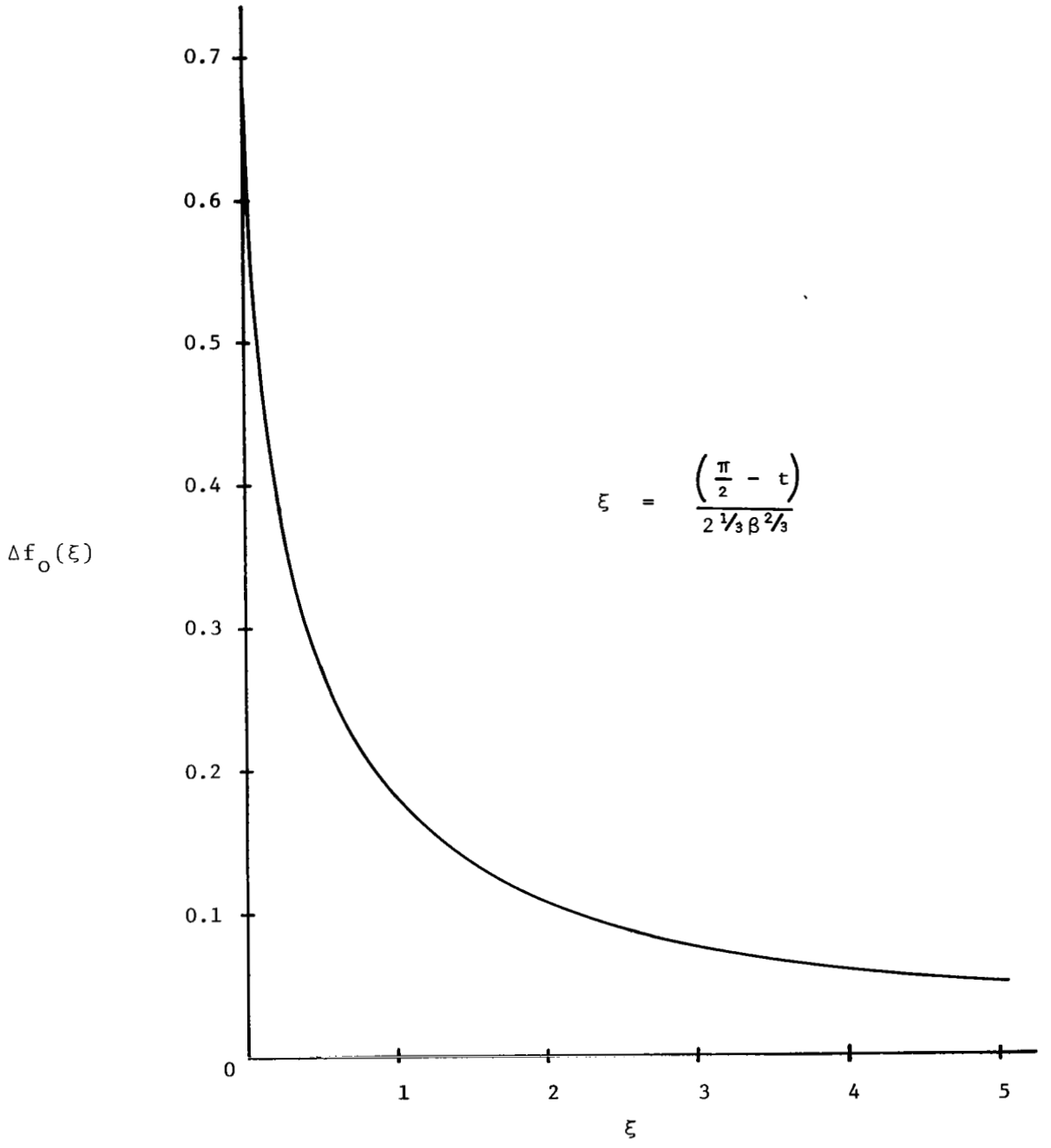

FIGURE 8. DEFINITION OF THE FUNCTION $\Delta f_o(\xi)$

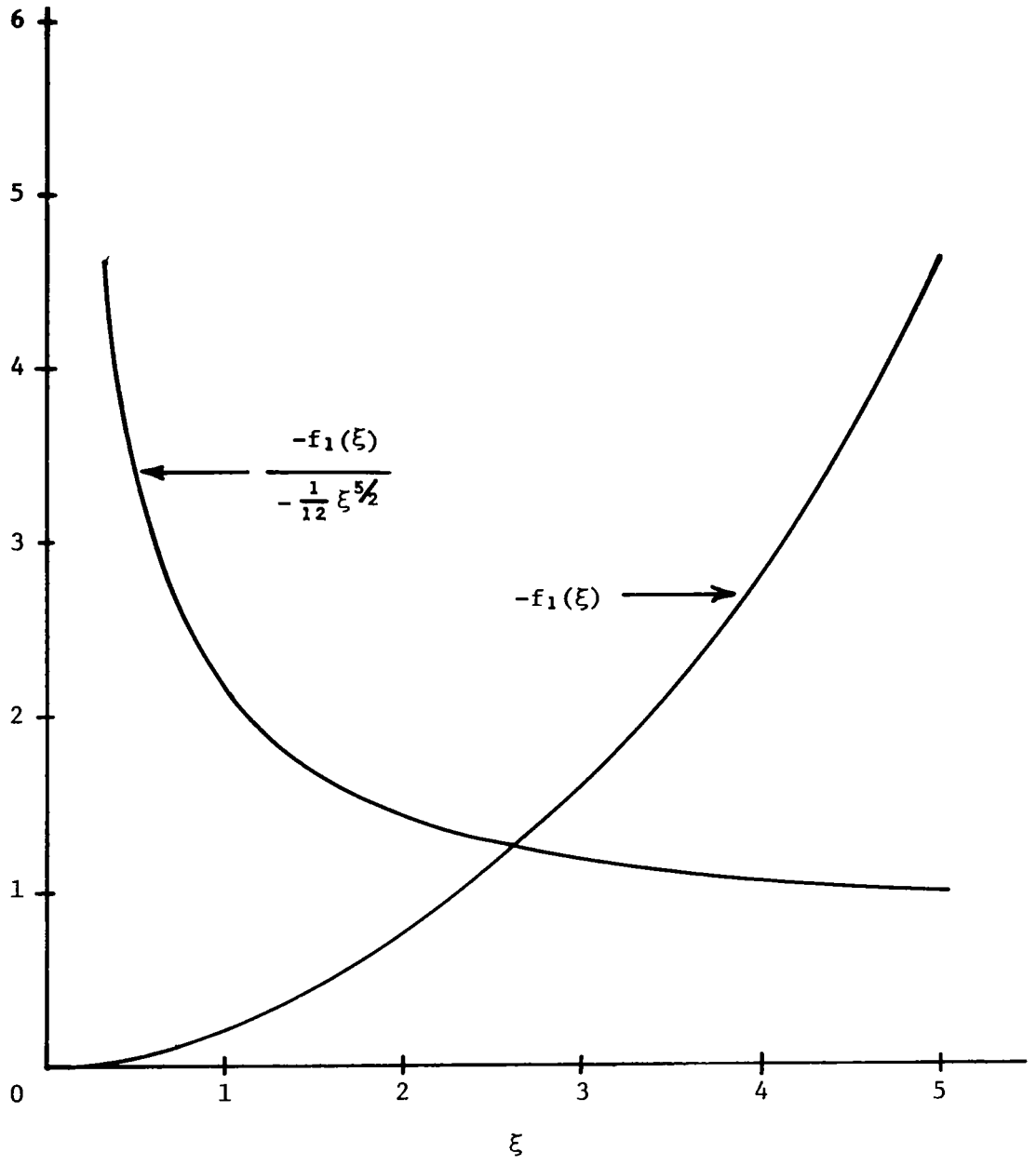

FIGURE 9. SOLUTION OF THE FUNCTION $f_1(\xi)$

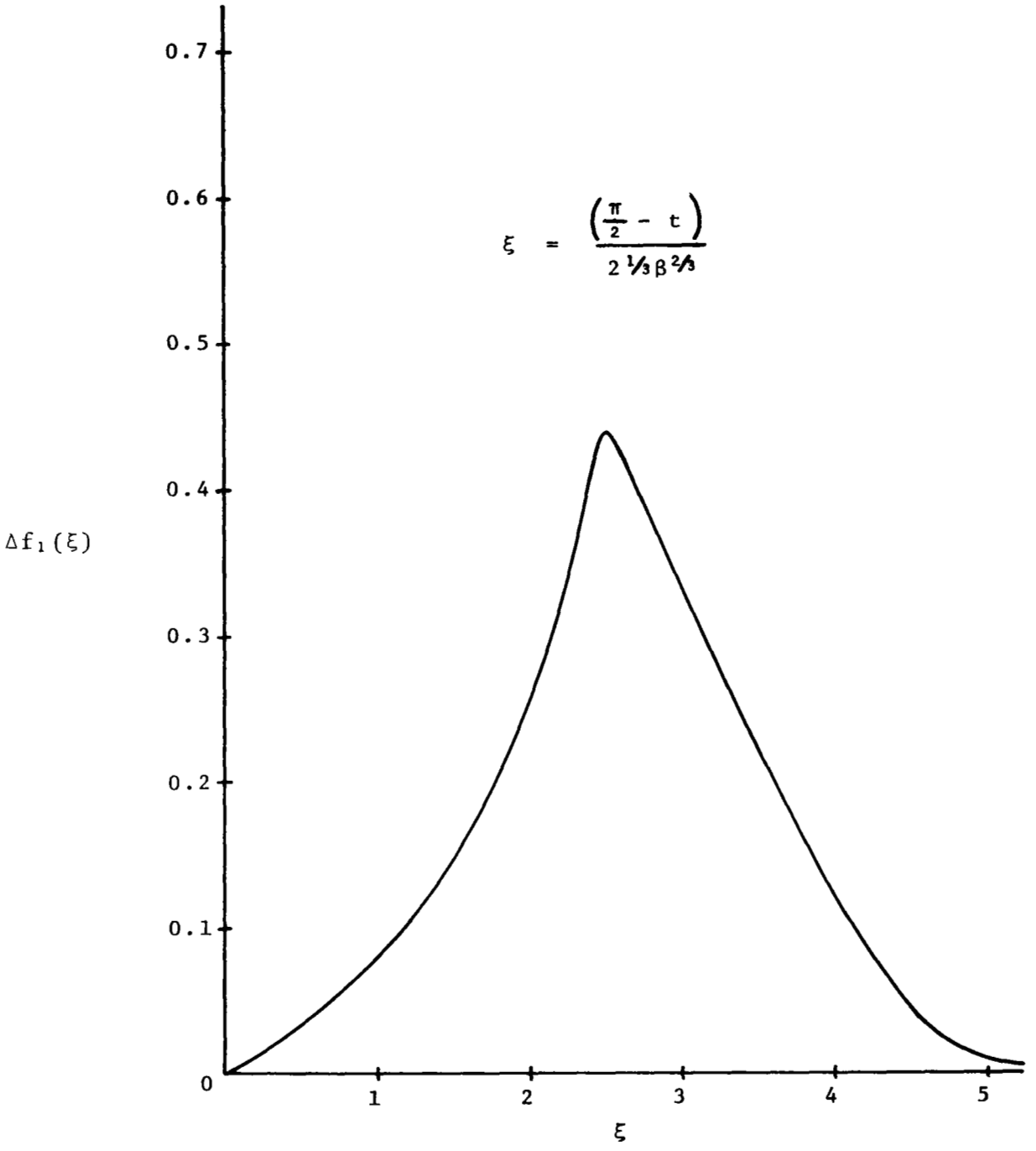

FIGURE 10. DEFINITION OF THE FUNCTION $\Delta f_1(\xi)$